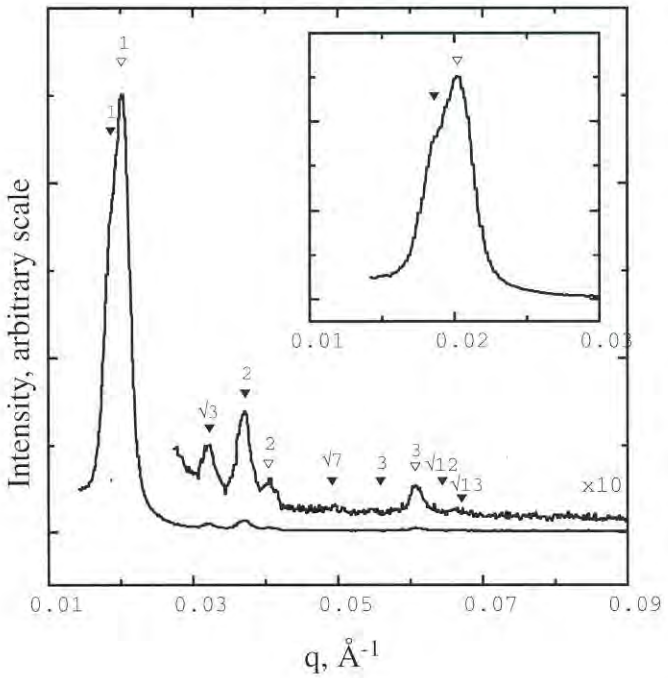

Figure 4: SAXS pattern for the ϕ = 0.54 solution in DEP showing the coexisting lamellar and hexagonal phases.

extremely narrow, probably on the order of 1°C wide, whereas in this case the interval is as much as 40°C. This is presumably attributable to the subtle balance of chain stretching, packing frustration, and conformational asymmetry that ultimately determines the precise location of the phase boundary.

Summary

The addition of solvents of varying selectivity to a styrene-isoprene diblock copolymer reveals a rich array of lyotropic and thermotropic transitions. The sequence of ordered phases may be approximately anticipated by the concept of diagonal trajectories on the melt phase map, but important distinctions are also exposed.

Acknowledgements

This work was supported in part by the National Science Foundation through award DMR-9528481.

References

[1] Bates, F.S. and Fredrickson, G.H., *Annu. Rev. Phys. Chem.* (1990) **41**, 525.

[2] Hamley, I.W., in *The Physics of Block Copolymers* (Oxford University Press, Oxford, 1998).

[3] Hanley, K.J. and Lodge, T.P., *J. Polym. Sci., Polym. Phys. Ed.* (1998) **36**, 3101.

[4] Fredrickson, G.H. and Bates, F.S., *Annu. Rev. Mater. Sci.* (1996) **26**, 503.

[5] Khandpur, A.K., Förster, S., Bates, F.S. *et al.*, *Macromolecules* (1995) **25**, 8796.

[6] Winey, K.I., Gobran, D.A., Xu, Z. *et al.*, *Macromolecules* (1994) **27**, 2392.

[7] Matsen, M.W. and Bates, F.S., *Macromolecules* (1996) **29**, 1091.

[8] Matsen, M.W., *Phys. Rev. Lett.* (1995) **74**, 4225.

[9] Hajduk, D.A., Takenouchi, H., Hillmyer, M.A. *et al.*, *Macromolecules* (1997) **30**, 3788.

[10] Hong, K.M. and Noolandi, J., *Macromolecules* (1983) **16**, 1083.

[11]Fredrickson, G.H. and Leibler, L., *Macromolecules* (1989) **22**, 1238.

[12] Olvera de la Cruz, M., *J. Chem. Phys.* (1989) **90**, 1995.

[13] Lodge, T.P., Pan, C., Jin, X. *et al.*, *J. Polym. Sci., Polym. Phys. Ed.* (1995) **33**, 2289.

[14] Lodge, T.P., Xu, X., Ryu, C.Y. *et al.*, *Macromolecules* (1996) **29**, 5955.

[15] McConnell, G.A. and Gast, A.P., *Macromolecules* (1997) **30**, 435.

[16] Hamley, I.W., Pople, J.A. and Diat, O., *Colloid Polym. Sci.* (1998) **276**, 446.

The Crystal Structure and Hydrogen Bonding System in Cellulose from Neutron Fibre Diffraction Data

P. Langan[1*], Y. Nishiyama[2] and H. Chanzy[3]

* Author for correspondence.
1 B Division, Los Alamos National Laboratory, MS-M888, Los Alamos NM 87545 USA. (http://lsdiv.lanl.gov/nsb)
2 Graduate School of Agricultural and Life Science, The University of Tokyo, Yayoi, Tokyo 113, 8657 Japan.
3 Centre de Recherches sur les Macromolécules Végétales, CNRS, affiliated with the Joseph Fourier University of Grenoble, BP 53, 38041 Grenoble Cedex 9, France.

Cellulose is a linear poly (1-4) β-D glucan which is normally biosynthesised as slender rod-like crystalline microfibrils acting as structural elements in plant cell walls and various other living organisms. The chemical and chain structure of cellulose was established by the 1930s using classical organic chemistry and developing polymer studies. A key feature of this structure is the presence of three hydroxyl groups on each glycosyl monomer; two secondary and one primary alcohol. The potential cohesive interchain hydrogen bonding of these hydroxyl groups provided an explanation for some surprising chemical and physical properties specific to cellulosic materials. It was also realised that one of the secondary alcohols, and possibly the primary alcohol, could form intrachain hydrogen bonds between adjacent glycosyl monomers, producing a planar chain conformation with 2_1 symmetry [1].

The crystalline nature of cellulose was revealed nearly 90 years ago when Nishikawa and Ono recorded the first X-ray patterns from fibre bundles from various plants [2]. X-ray diffraction has become a standard tool for studying cellulose fibres, allowing classification of the various celluloses into a number of crystalline allomorphs [3,4]. Cellulose is crystallised into a metastable form during biosynthesis. Native cellulose, or cellulose I, can be made to undergo an irreversible transition to a stable form, cellulose II, by two distinct processes: regeneration and mercerisation. Regeneration involves either preparing a solution of cellulose in an appropriate solvent or of an intermediate derivative followed by coagulation and recrystallisation. Mercerisation involves intra-crystallline swelling of cellulose in concentrated aqueous NaOH followed by washing and recrystallisation. A number of other cellulose polymorphs can be obtained by physical or chemical modification, in particular cellulose III and cellulose IV [5,6]. These processes have been commonly used in industrial preparations in order to improve mechanical properties and reception to dye.

One of the first detailed molecular models for cellulose I was proposed in 1937 and consisted of antiparallel chains packed into a monoclinic cell [7]. However subsequent studies on cellulose from a variety of sources using different diffraction techniques have produced a number of different unit cells and ways of packing cellulose chains into these cells. In particular, electron diffraction from *Valonia* cellulose taken by Honjo and Watanabe contained spots that could not be indexed by the conventional two-chain unit cell [8]. They proposed an eight-chain unit cell to explain the diffraction pattern. The development of high-resolution ^{13}C solid state NMR techniques in the 1980s has brought a new dimension to the determination of the crystal structure of cellulose. The ^{13}C NMR spectra of highly crystalline cellulose such as that of *Valonia* showed unambiguously the presence of two crystalline allomorphs in cellulose I, namely cellulose Iα and cellulose Iβ [9,10]. On the other hand, the Iβ allomorph was found to be the predominant form in tunicin, another highly crystalline cellulose sample from animal origin [11]. Cellulose from *Glaucocystis* has been shown to consist of essentially cellulose Iα [12, 13].

It is now recognised that cellulose has characteristics that allow the formation of unique cellulosic structures within specific species and often within different tissues of the same organism [14]. The species specific compositional ratio of cellulose Iα and Iβ and also the relative distribution of cellulose Iα and Iβ domains in biosynthesised microfibrils is thought to affect structure, properties and function. Some fungal cellulases have enhanced activity on substrates of specific cellulose Iα/Iβ composition. These developments indicate that the crystal and molecular structures of cellulose I have to be revised in light of this dimorphism. Electron diffraction studies have recently shown the Iα and Iβ forms to correspond to one-chain triclinic and two-chain monoclinic unit cells, respectively [15]. A combination of biochemical techniques and electron microscopy have allowed the polarity of the chains packed in these cells to be determined [16]. A priority now is to obtain new X-ray and neutron diffraction data from pure Iα and Iβ fibres, in order to determine precise atomic coordinates for these allomorphs.

There has also been controversy over the unit cell of cellulose II. The X-ray structure, determined from diffraction studies on regenerated fibres, has defined the crystals of this polymorph as consisting of two antiparallel and crystallographically independent chains [17, 18]. The case of mercerised cellulose is less clear. Some authors believe that in the cellulose II crystals obtained by mercerisation the chains are antiparallel [19]. This is contradicted by other authors who propose a parallel-chain system, because of the topographical problems involved in converting from a parallel-chain cellulose I to an antiparallel-chain cellulose II [20, 21]. The antiparallel X-ray structure has a monoclinic unit cell where the chains are aligned on the two-fold screw axis of the cell. Both chains have equivalent backbone and sugar conformations but differ in the conformation of their primary alcohol (commonly called hydroxymethyl groups); *gt* for the chain located at the cell origin and *tg* for the centre chain [22]. This model has been challenged by observations resulting from a number of ^{13}C NMR studies. In the cellulose II spectra, the C6 resonance occurs as a singlet near 64ppm and not as the expected doublet with resonances near 64 and 66ppm if both *gt* [23-27] and *tg* conformations are coexistent in the crystalline structure [17-19].

The model of cellulose II has been further challenged by the recent determination of the crystalline structures of two cellulose oligomers, β-cellotetraose [28, 29] and methyl β-cellotrioside [30] that are known to crystallise in the same type of lattice as cellulose II. Their molecular configurations are similar to that of the cellulose II model except in two main respects; all hydroxymethyl groups are in the *gt* conformation and the sugar and backbone conformations are slightly different for the two chains. On the basis of these observations it is clear that the structure of cellulose II should also be re-examined.

Another important feature of all the crystalline cellulose allomorphs that needs to be re-examined is that of the hydrogen bonding system. There are significant differences in the hydrogen bonding schemes proposed for β-D cellotetraose by Gessler *et al.* [28] and Raymond *et al.* [29]. Recent MD simulations [31] would appear to support the scheme proposed by Gessler *et al.* Both these hydrogen bonding schemes differ from any potential hydrogen bonding network in the structure of cellulose II determined in the earlier fibre diffraction studies [17,18]. A resolution of the hydrogen bonding scheme in cellulose II and the determination of hydrogen bonding schemes in the other cellulose allomorphs is necessary for an understanding of the structure, reactivity and properties of cellulose in its various forms and the processes involved in conversion from one form to another.

The power of neutron fibre diffraction for locating hydrogen atoms [32] and investigating hydrogen bonding [33, 34] has already been demonstrated. Compared to oxygen and carbon, hydrogen is a weak scatterer of X-rays, but not of neutrons. The scattering length of hydrogen for neutrons is negative, but it is positive and of comparable magnitude for deuterium, carbon and oxygen (-0.37×10^{-12}cm for H, 0.667×10^{-12}cm for D, 0.665×10^{-12}cm for C and 0.58×10^{-12}cm for O) [35]. At the resolution of most fibre diffraction studies, where individual atoms cannot be resolved, the scattering length of hydrocarbon and hydroxyl groups is small (0.291×10^{-12}cm for CH, -0.083×10^{-12}cm for CH_2 and 0.206×10^{-12}cm for OH), but of deuteroxyl groups is large (1.245×10^{-12}cm). It has already been shown that, in cellulose-II, a partial replacement of the OH moieties by OD can lead to meaningful neutron fibre diffraction patterns where a substantial contrast can be observed when comparing data from the deuterated and hydrogenated forms [36]. Unfortunately, in this earlier work, the substitution of OH by OD was only partial and the fibres poorly oriented so that the exact positions of these moieties within the lattice could not be determined.

We are involved in a long term study using neutron and synchrotron X-ray techniques to determine the precise structures of the various cellulose polymorphs. Here we report on the first results from our neutron diffraction studies. We have developed methods for replacing H atoms involved in hydrogen bonding in cellulose fibres with D, without any loss in crystalline perfection [37,38]. The deuterated fibres give high resolution neutron diffraction patterns with intensities that are substantially different from the intensities observed in neutron fibre diffraction patterns obtained from hydrogenated fibres. So far we have collected neutron diffraction data from the deuterated and hydrogenated forms of cellulose Iβ, cellulose Iα/Iβ and cellulose II. Measured intensities from these diffraction patterns are being used to compute Fourier difference maps

leading to full descriptions of the hydrogen bonding systems. In this report we present the results of our first full analysis: the hydrogen bonding system in cellulose II.

Neutron Fibre Diffraction Patterns

Neutron diffraction data were collected on diffractometer D19 at the Institut Laue Langevin, Grenoble, using generic data collection strategies that have been described elsewhere [38]. Cellulose Iβ samples were prepared from the cellulosic mantles of tunicates (*Halocynthia roretzi*) and cellulose Iβ+Iα samples from the walls of green algae (*Cladophora sp.*). The proportion of Iα and Iβ in *Cladophora* is approximately 3:1. Cellulose II samples were prepared from flax fibres. Preparing highly crystalline, hydrogenated and deuterated, samples large enough for neutron diffraction required a number of innovative steps that have been described elsewhere [37, 39]. Neutron diffraction patterns are shown in Figures 1(a)-(f). Figures 1(a), (c) and (e) correspond to diffraction from hydrogenated samples and Figures 1(b), (d) and (f) to diffraction from deuterated samples.

Figures 1(a) and 1(b) correspond to cellulose Iβ (*Halocynthia*). Diffraction features from both the hydrogenated and deuterated samples extend well beyond atomic resolution (0.9Å). Several hundred diffraction spots can be measured, far exceeding the number of data available from reported X-ray fibre diffraction studies of cellulose I. A comparison of hydrogenated and deuterated patterns (Figures 1(a) and 1(b)) reveals substantial differences in the relative distribution of intensity, in particular on the first, third, fourth, seventh and eighth layerlines. Figures 1(c) and 1(d) correspond to cellulose Iα+Iβ (*Cladophora*). The resolution of the data in these diffraction patterns is similar to that from Iβ. The patterns from *Cladophora* and *Halocynthia* show a great deal of similarity. Differences can nevertheless be seen in the third and fifth layer lines in the patterns from deuterated samples (Figures 1(b) and 1(d)). Figures 1(e) and 1(f) correspond to cellulose II. The difference between the patterns are striking particularly along the fibre axis where the deuterated pattern presents a strong 002 meridional which is totally absent from the hydrogenated pattern. There are also large differences on the first, second and fifth layer lines. Diffraction features extend to a resolution of ~1.2Å.

The neutron diffraction patterns we have recorded extend to a much higher resolution than any X-ray diffraction patterns from cellulose published so far. In fact, the resolution of the patterns from *Halocynthia* and *Cladophora* matches closely that of electron diffraction diagrams obtained on 1 micron of carefully selected specimens [40]. With electron diffraction, however, it is not yet possible to establish with certainty the relation between the intensity of the diffraction spots and the structure factors. The intensities measured from these neutron diffraction patterns are being used to determine the crystal structure and hydrogen bonding in cellulose. We have just completed a full analysis of the cellulose II data [41], the results of which are represented below.

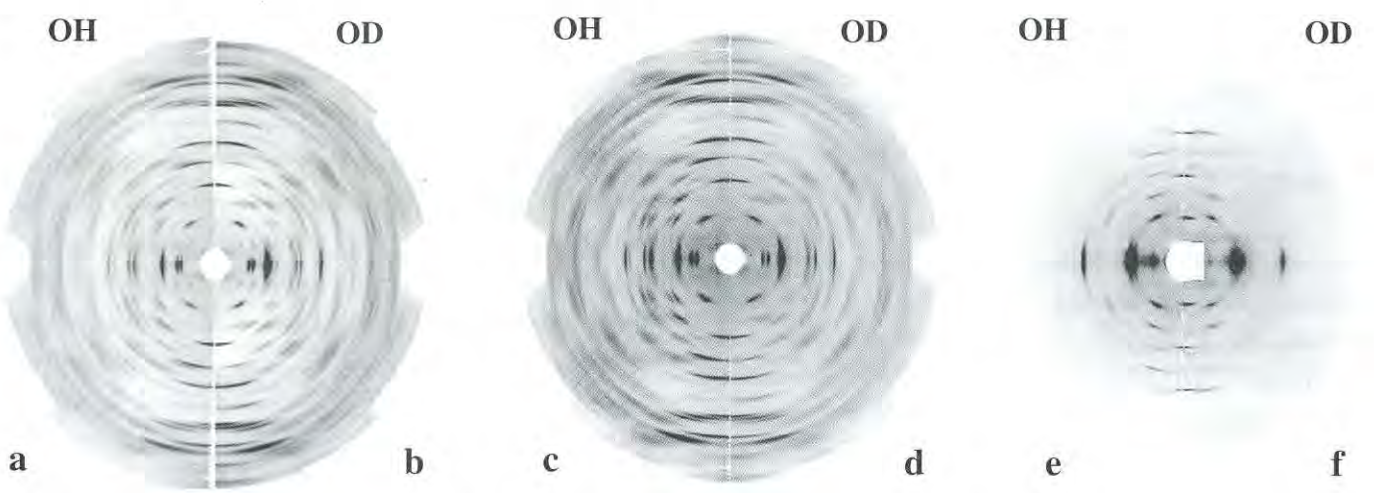

Figure 1: Series of neutron fibre diffraction patterns for cellulose I and cellulose II with vertical fibre axes and printed at the same camera length; (a) from a reconstituted sample of tunicin (cellulose Iβ) microcrystals; (b) as in (a), but after substituting all OHs by ODs; (c) from a reconstituted sample of *Cladophora* cellulose (cellulose Iα+Iβ); (d) as in (c) but after substitution of OHs by ODs; (e) from mercerized flax in standard $NaOH/H_2O$; (f) as in (e), but mercerized in $NaOD/D_2O$.

A Revised Structure and Hydrogen Bonding System for Cellulose II [41]

Measured intensities from neutron diffraction data collected from cellulose II have been combined with phases calculated from an X-ray model in order to compute Fourier difference maps leading to a full description of the hydrogen bonding system. In fact, since there are two competing models in the literature we decided to re-refine the structure of cellulose II against the X-ray data. Both models agree on several points, namely that the structure of cellulose II is based on a two chain unit cell where the chains are antiparallel and that the chains are located on the 2_1 axes of the monoclinic cell. In model A the chains have different conformations for their hydroxymethyl groups [17, 18]. In model B, derived from the crystal and molecular structure of cellulose oligomers, the hydroxymethyl groups are in the same conformation for both chains [28, 29]. The carbon and oxygen atom positions of both models were refined against the X-ray fibre diffraction data allowing the sugar and backbone geometries of the independent chains to change. We could not differentiate between the resulting two models on the basis of their agreement with the X-ray data alone. The H/D atom positions of both models identified in the neutron Fourier difference maps were then refined against our neutron diffraction data. Model B was in significantly better agreement with the data than model A and we were able to reject model A. A final 2Fd-Fc map is shown in Figure 2. Model B has the same basic conformational features as molecules in crystals of β-D cellotetraose. In particular the two chains have different backbone and sugar conformations. The sugar of the central chain is strained and the chains are displaced relative to each other by ~0.24c. In both the Fd-Fh and 2Fd-Fh Fourier maps there is a difference density feature that cannot be assigned to a deuterium atom. This peak, identified by an arrow in Figure 2(a), is in a position that would be occupied by a hydroxymethyl group near the *tg* position. Allowing the hydroxymethyl group of the central chain to be shared between *tg* and *gt* positions significantly improved the agreement with data and indicated an occupancy of 30% and 70% respectively. It is interesting to note that in MD simulations the hydroxymethyl groups are not exclusively in the *gt* conformation [31]. The hydrogen bonding system is shown schematically in Figure 3. A systematic three-centre intrachain hydrogen bond [42] is observed in both chains. This bond has a major component between O3 and O5,

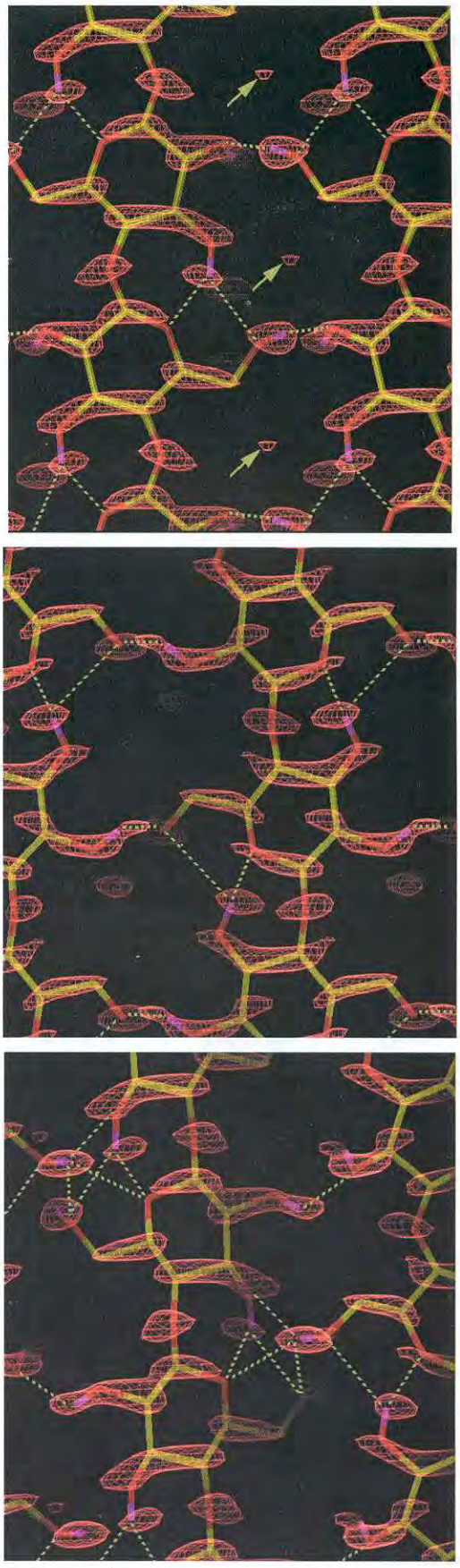

Figure 2: The final 2Fd-Fc map (red density) for model B', showing views of the planes containing a) the centre chains b) the origin chains and c) origin and centre chains. Cellulose chains are represented by a skeletal model in which carbon atoms are yellow, oxygen atoms are red and labile hydrogen atoms are pink. Hydrogen atoms covalently bonded to carbon are not depicted. The arrows in a) indicate density peaks which could not be accounted for by labile hydrogen atom positions. The potential hydrogen bonds are represented by broken lines.

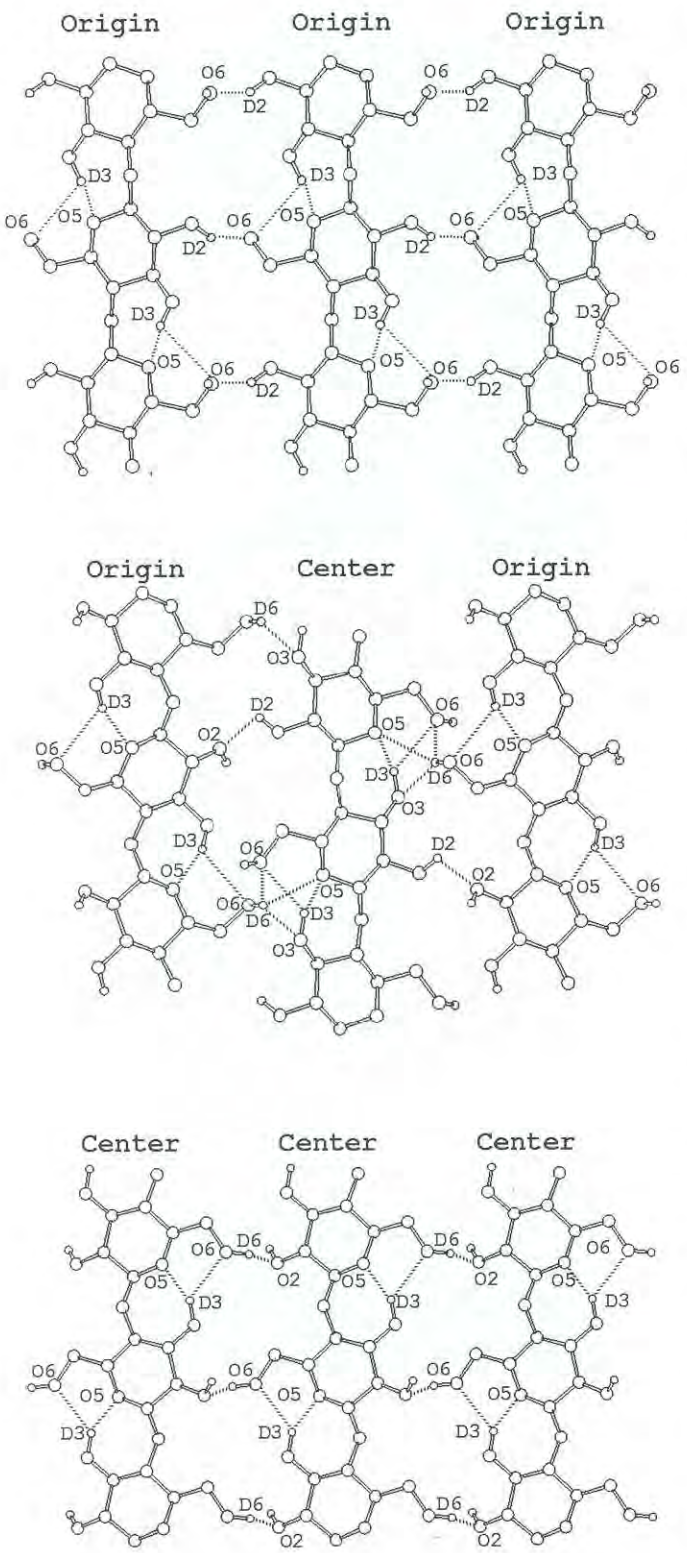

Figure 3: A schematic representation of the hydrogen bonds in cellulose II. Only atoms involved in hydrogen bonding are labeled. Hydrogen bonds are represented by dotted lines. Intermolecular hydrogen bonds are O2-D...O6 in sheets containing only origin molecules and O6-D...O2 in sheets containing only centre molecules. In the sheet containing both centre and origin molecules there are O6-D...O6 and O2-D...O2 intermolecular hydrogen bonds. The former has minor components involving O5 and O3 as acceptors. Intramolecular hydrogen bonds are O3-D...O5 in each molecule with a minor component involving O6 as acceptor.

with O3 as donor. A similar three-centre hydrogen bond interaction is observed in the β-D cellotetraose structures [28, 29]. The intermolecular hydrogen bonding differs substantially from that observed in β-D-cellotetraose. One consequence of this difference is that O6 of the origin chain can donate a hydrogen bond to three possible acceptors, the major component being to O6 of the centre chain. These three acceptors already interact with each other through a three-centre hydrogen bond. It is unclear to what extent disorder of the O6 group of the centre chain is responsible for this intricate hydrogen bonding arrangement.

Conclusion

Our study on cellulose II has provided, for the first time, a reliable set of coordinates for all of the atoms, including hydrogen, in the crystal structure of cellulose II. A similar analysis of the neutron diffraction data collected from cellulose Iβ (*Halocynthia*) and cellulose Iα+Iβ (*Cladophora*) is under way. We are also in the process of collecting neutron diffraction data from the newly discovered cellulose from *Glaucocystis* which has been shown to be essentially cellulose Iα [12, 13] and also cellulose III. It has been said that in the history of polymer science, cellulose has most often been a trailblazer, advancing many analytical methods such as crystallography and microscopy [43, 44]. These neutron diffraction studies are providing the first three dimensional descriptions of hydrogen bonding systems in fibrous polysaccharides. They are also driving the development of new instrumentation such as the Neutron Diffraction Structural Biology Station being built at Los Alamos, New Mexico [45].

Acknowledgements

We thank the Institut Laue Langevin for the provision of neutron beamtime. Y.N. thanks the French Government and the Japanese Society for the Promotion of Science for financial support.

References

[1] Hermans, P.H., *Physics and Chemistry of Cellulose Fibers* (Elsevier, New York, 1949).

[2] Nishikawa, S. and Ono, S., *Proc. Tokyo. Math. Phys. Soc.* (1913) **7**, 131.

[3] Roelofsen, P.A., *The Plant Cell-Wall* (Gebruder Borntraeger, Berlin, 1959).

[4] Davis, W.E., Barry, A.J., Peterson, F.C. and

King, A.J., *J. Am. Chem. Soc.* (1943) **65**, 1294.
[5] Krassig, H.A., *Cellulose, Structure, Accessibility and Reactivity* (Gordon and Breach Pub., Yverdon, Switzerland, 1993).
[6] Hess, K. and Kiessig, H., *Z. Phys. Chem. Abt. B* (1941) **49**, 235.
[7] Meyer, K.H. and Misch, L., *Helv. Chim. Acta* (1937) **20**, 232.
[8] Honjo, G. and Watanabe M., *Nature* (1958) **181**, 326.
[9] Atalla, R.H. and VanderHart, D.L., *Science* (1984) **223**, 283.
[10] VanderHart, D.L. and Atalla, R.H., *Macromolecules* (1984) **17**, 1465.
[11]Belton, P.S., Tanner, S.F., Cartier, N. and Chanzy, H., *Macromolecules* (1989) **22**, 1615.
[12] Sugiyama, J., Persson, J. and Chanzy, H., *Macromolecules* (1991) **24**, 2461.
[13] Imai, T., Sugiyama, J., Itoh, T. and Horii, F., *J. Struct. Biol.* (in press).
[14] Atalla, R.H., in *Comprehensive Natural Products Chemistry* (Ed. B.H. Piuto), Volume 3 (Elsevier, Cambridge 1999).
[15] Sugiyama J, Vuong R, and Chanzy H., *Macromolecules* (1991) **24**, 4168.
[16] Koyama, M., Helbert, W, Imai T., Sugiyama J. and Henrissat, B., *Proc. Natl. Acad. Sci.* (1997) **94** , 9091.
[17] Kolpak, K.J. and Blackwell, J., *Macromolecules* (1976) **9**, 273.
[18] Stipanovic, A. and Sarko, A., *Macromolecules* (1976) **9**, 851.
[19] Kolpak, K.J., Weih, M. and Blackwell, J., *Polymer* (1978) **19**, 123-131.
[20] Fengel, D., *Das Papier* (1993) **12**, 695.
[21] Kroon-Batenburg, L.M.J., Bouma B. and Kroon, J., *Macromolecules* (1996) **29**, 5695.
[22] The conformation of the hydroxymethyl group is defined by two letters, the first referring to the torsion angle c (O5-C5-C6-O6) and the second to the torsion angle c' (C4-C5-C6-O6). Thus, an ideal *gt* conformation would be defined as the set of two angles : 60°, 180°.
[23] Dudley, R.L., Fyfe, C.A., Stephenson, P.J., Deslandes, Y., Hamer, G.K. and Marchessault, R. H., *J. Am. Chem. Soc.* (1983) **105**, 2469.
[24] Fyfe, C.A., Stephenson, P.J., Veregin, R.P., Hamer, G. and Marchessault, R.H., *Carbohydr. Chem.* (1984) **3**, 663.
[25] Isogai, A., Usuda, M., Kato, T., Uryu, T. and Atalla, R.H., *Macromolecules* (1989) **22**, 3168.
[26] Horii, F., Hirai, A., Kitamaru, R. and Sakurada, I., *Cellulose Chem. Technol.* (1985), **19**, 513.
[27] Horii, F., Hirai, A., Kitamaru, R. and Sakurada, I., *Polym. Bull.* (1983) **10**, 3168.
[28] Gessler, K., Krauss, N., Steiner, T., Betzel, C., Sandman, C. and Saenger, W., *Science* (1994) **266**, 1027.
[29] Raymond, S., Heyraud, A., Tran Qui, D., Kvick, Å. and Chanzy, H., *Macromolecules* (1995) **28**, 2096.
[30] Raymond, S., Henrissat, B., Tran Qui, D., Kvick, Å. and Chanzy, H., *Carbohydr. Res.* (1995) **277**, 209.
[31] Kroon-Batenburg, L.M.J., Kroon, J., *Glycoconjugate J.* (1997) **14**, 677.
[32] Shotton, M.W., Pope, L.H., Forsyth, V.T., Langan, P., Denny, R.C., Giesen, U., Dauvergne, M-T. and Fuller, W., *Biophys. Chem.* (1997) **69**, 85.
[33] Mahendrasingam, A., Al-Hayalee, Y., Forsyth, V.T., Langan, P., Fuller, W., Oldman, R.J., Blundell, D.J. and Mason, S. A., *Physica B* (1992) **180&181**, 528.
[34] Langan, P., Forysth, V.T., Mahendrasingam, A., Pigram, W.J., Mason, S.A. and Fuller, W., *J. Biomol. Struct. Dyn.* (1992) **10**, 489.
[35] Koester, L. and Rauch, H., *Summary of Neutron Scattering Lengths*, IAEA contract 2517/Rb (International Atomic Energy Agency, Vienna, 1981).
[36] Langan, P., Denny, R.C., Mahendrasingam, A., Mason, S.A., Jaber, A., *J. Appl. Cryst.* (1996) **29**, 383.
[37] Nishiyama, Y., Isogai, A., Okano, T., Müller, M. and Chanzy, H., *Macromolecules* (1999) **32**, 2078.
[38] Nishiyama, Y., Okano, T., Langan, P. and Chanzy, H., *Int. J. Biol. Macromol.* (1999) **26**, 279.
[39] Nishiyama, Y., Kuga, S., Wada, M. and Okano, T., *Macromolecules* (1997) **30**, 6395.
[40] Favier, V., Chanzy, H. and Cavaillé, J-Y., *Macromolecules* (1995) **28**, 6365.
[41] Langan, P., Nishiyama, Y. and Chanzy, H., *J. Am. Chem. Soc.* (1999) **121**.
[42] Jeffrey, G.A. and Saenger, W., *Hydrogen Bonding in Biological Structures* (Springer Verlag, Berlin, 1991).
[43] Marchessault, R.H. and Sundararjan, P.R., in *The Polysaccharides* (Ed. G. Aspinall), Volume 2 of Molecular Biology (Academic Press, New York, 1983).
[44] O'Sullivan, A., *Cellulose* (1997) **4**, 173.
[45] See http://lsdiv.lanl.gov/nsb and Schoenborn, B.P. and Langan, P., *Biophys. J.* (1999) **76**, A392.

Chromatin Higher-Order Structure: Results from Small-Angle X-Ray Scattering and Histone-Octamer Crystallography

J. Kilner[1], J.M. Nicholson[2], L. Chantalat[3], S.J. Lambert[4], H.W Rattle[5] and J.P. Baldwin[4]

1 MAFF, York, U.K.
2 Daresbury Laboratory, Daresbury, Warrington, Cheshire WA4 4AD, U.K.
3 Laboratoire de Crystallographie Macromoleculaire, Institut de Biologie Structurale, 41 Avenue des Martyrs, 38027 Grenoble 1, Cedex, France.
4 Biophysics Group, School of Biomolecular Sciences, John Moores University, Byrom Street, Liverpool L3 3AF, U.K.
5 Biophysics Laboratories, University of Portsmouth, White Swan Road, Portsmouth PO1 2QX, U.K.

Introduction

Chromatin is the highly ordered DNA-protein complex, which serves to package and organise the chromosomal DNA in the cell nucleus. It is able to alter the level of DNA packaging, thus playing crucial roles at different stages of the cell cycle. The nucleosome core is the basic unit of chromosome structure, composed of a species-dependent 168 - 240 base pairs of DNA, 146 of which are wound around an octameric histone-protein core containing two dimers of histone proteins, 2(H2A.H2B), complexed with a tetramer of histones, $(H3.H4)_2$. A fifth histone, the linker histone H1 (also H5 in avian erythrocytes), binds to the DNA outside the complex containing the core. The complex of the nine histones plus 168-240 base pairs of DNA is the nucleosome.

The histones are very highly conserved between relatively unrelated species, even between plants and animals, which highlights their crucial role in the chromosome and suggests that all histones are evolutionarily related.

Nucleosomes are strung together over the whole of the DNA in the cell nucleus and form zig-zags in a long chain. The zig-zagging chain folds into a higher-order structure, which is accepted to be a left-handed coil of about six nucleosomes per 10nm and of diameter ~30nm.

Many studies of higher-order structure have been carried out since electron microscopy suggested the existence of the 30nm coil. Perhaps the most notable have been the use of neutron-small-angle contrast variation to show that the histone H5 is on the inside of the structure [1, 2] and optical-transform studies of electron microscopy images showing a left-handed coiled structure [3]. Fibre-diffraction studies, although useful in establishing a 10nm repeat along the fibre [4] and packing of the coils in the fibre [5], have not produced diffraction to high resolution and models for the arrangement of nucleosomes in the core particle abound. Two models seem to have most credibility; the first being where the nucleosomes form the coil and the DNA goes from one nucleosome to the next *around* the coil [6]. The second model is where the nucleosomes interlace back and forth *across* the coil [7].

There are several recent reviews of this field of work [8], but a most crucial missing piece of information is the location of the linker histone which was thought to be located more or less symmetrically at the diad axis of the nucleosome, protecting the DNA from nuclease attack as it enters and as it leaves after two-turns around the octamer histone core [9]. Neutron-scattering results [10, 11] showed that the linker histone has a lower radius from the centre of the histone octamer than would be suggested by such a model and more recently several studies confirm an asymmetric location of linker histones [12].

Results

Small-Angle X-Ray Scattering

One of the problems in studying the higher-order coil of nucleosomes by small-angle scattering is that fractionation of the chains of forty or more nucleosomes needed for the studies (cleaved as polynucleosomes out of cell nuclei by light micrococcal nuclease digestion) can disturb the linker histones. Therefore a method was developed for gently fractionating chick-erythrocyte polynucleosomes on a Sephacryl 1000 column.

X-ray small-angle scattering spectra for non-aggregating "rods" of molecules in solution are analysed by plotting the graph of $sI(s)$ versus s^2 where s is the scattering-angle-θ-dependent parameter $2.\sin\theta/\lambda$ and λ is the wavelength. $I(s)$ is the intensity of scattering, as a function of θ, measured in these experiments by the detector on beam-line 8.2 at the Daresbury Laboratory Synchrotron Radiation Source. The gradient of the graphs, if the rods are rigid and the scatter curves are concentration independent, is a measure of the

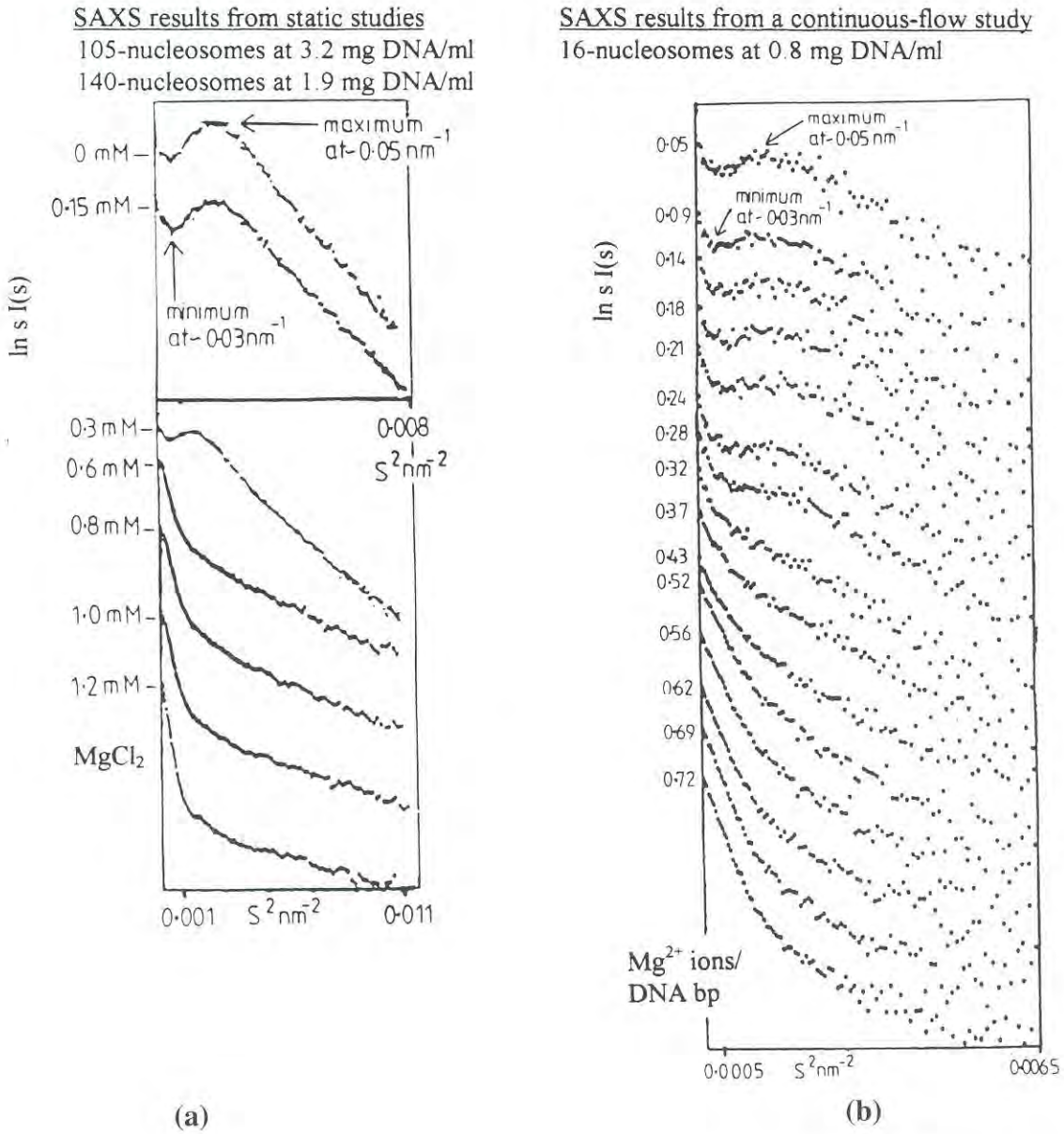

Figure 1: Magnesium-ion dependence of the scattering of X-rays, ln(s.I(s)) vs s^2, where I(s) is the intensity of scattering from solutions of nucleosome multimers. The scattering parameter s is related to the scattering angle 2θ by $s = 4\pi\sin\theta / \lambda$, where λ is the X-ray wavelength. The number of nucleosomes in the multinucleosomes was determined from agarose-gel electrophoresis of the DNA extracted from them, knowing the nucleosome repeat of 210 base pairs in chick erythrocytes. In the static study of Figure 1(a), the magnesium-ion molarity of each solution was known by the dilution used from a stock 1M solution of $MgCl_2$. In the continuous-flow experiment of Figure 1(b), a dialysis cell was used to continuously change and continuously monitor the concentration of magnesium ions. Note that at the end of the folding processes, at low s and the highest magnesium concentrations, the s.I(s) plots from the multinucleosomes showed straight line plots amenable to a rod-Guinier analysis for long chains of multinucleosomes such as in Figure 1(a) (see text) leading to Figures 2 and 3.

square of the cross-sectional radius of gyration. The intercept on the sI(s) axis gives the mass per unit length of the rods if the graphs are put on an absolute scale by calibration from the scattering curve of a standard, in this case scattering from nucleosome core particles. This analysis does not depend on the precise molecular weight of the rods provided the ratio of the length to diameter is greater than about two to three (surprisingly). These criteria were checked in the present experiments and did apply to Figure 1(a). All spectra were checked for any aggregation by photon-correlation spectroscopy studies of the folding pathways.

Figure 1 shows cross-sectional Guinier plots of the multinucleosomes in solution as a function of magnesium-ion concentration as the nucleosomes fold from a zig-zag chain and eventually into the 30nm coil [13]. The magnesium ions were introduced in a continuous way using a dialysis cell specially made for beamline 8.2 and Figure 1(b) shows the folding pathway most clearly, although

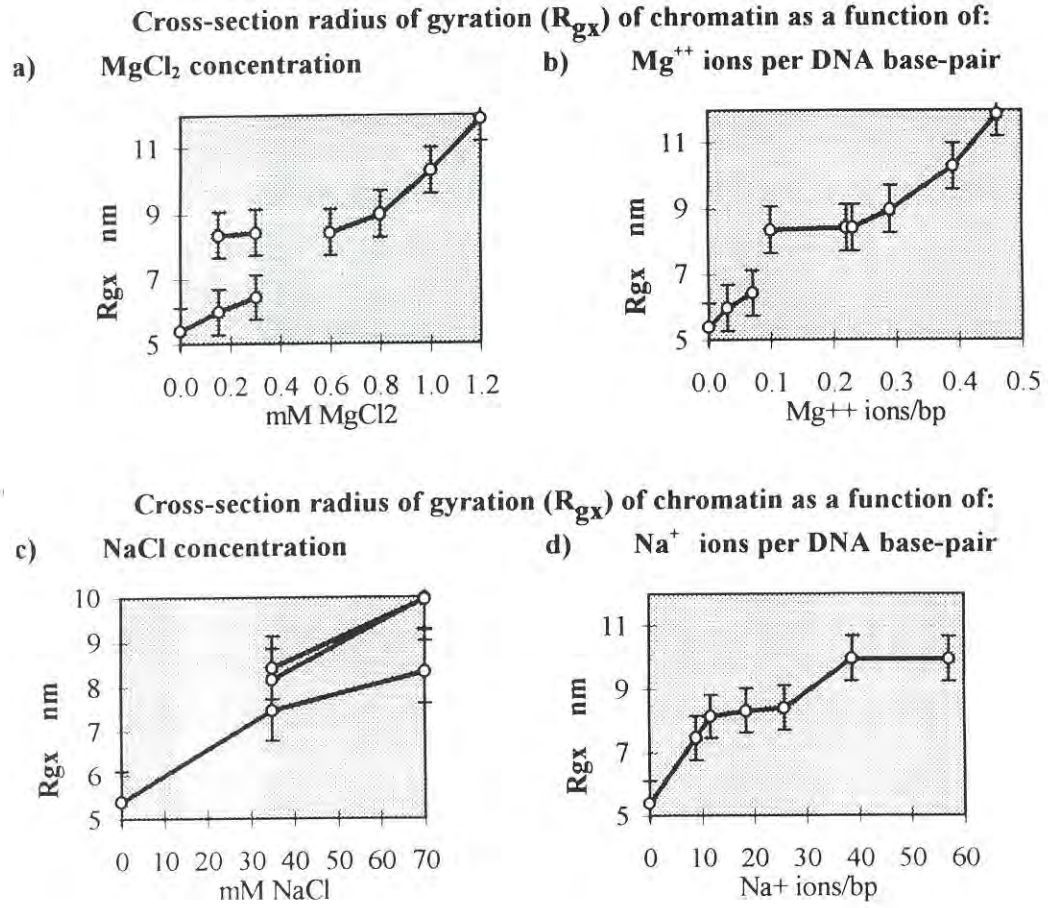

Figure 2: Comparison of the cross-sectional radii of gyration, R_{gx}, of multinucleosomes containing more than 100 nucleosomes, and their dependence on the concentrations of Na^+ and Mg^{2+} ions. The R_{gx} values come from the slopes of the rod-Guinier plots such as Figure 1(a). The curves of the R_{gx} values are more continuous when they are plotted against ions per base pair in the multinucleosomes, calculated from the known molecular weights and DNA concentrations.

these multinucleosomes had too few nucleosomes to carry out the full rod analysis for the scattering curves.

Figure 1(a) shows results for high multimers of nucleosomes where the length to diameter of the rods is high. Straight cross-section Guinier plots are observed near the finally compacted state. Cross-section radii of gyration and mass-per-unit-length values (expressed as numbers of nucleosomes per unit length by calibration of the plots against nucleosome core particles) are plotted against the concentration of Na^+ ions and Mg^{2+} ions in Figures 2 and 3 respectively. Knowing the molecular weight of the nucleosome multimers (from gels of the DNA extracted), the ion concentrations could be calibrated in terms of concentration of ions per base pair for the different measurements with samples at different concentrations of multinucleosomes.

It is clear from Figures 2 and 3 that the compaction of the higher-order coil of nucleosomes depends on the number of ions per base pair.

These studies show in addition that the compaction is greater in Mg^{2+} ions than in Na^+ ions and reaches 6 to 8 nucleosomes per 11nm length of coil with cross-sectional radii of gyration of 10 to 11 nm (coil cross-section diameter about 28 to 31nm). Continuous-flow conductivity measurements and photon-correlation experiments showed that the folding of the polynucleosomes at low ionic strength also was different in Na^+ ions compared with Mg^{2+} ions. Indeed folding in Mg^{2+} did not proceed at all in a fixed volume of sample until the concentration of the ions was typically 0.2 mM.

Histone-Octamer Crystallography

The histone octamer, 2(H2A.H2B).(H3.H4)2, was crystallised in 2M KCl/1.35M phosphate [14] giving a $P6_5$ space group with lattice parameters $a = b =$ 15.8 nm, c = 10.2nm. We solved the structure to 0.215 nm [14,15] resolution, from data collected on beamline 7.2 at Daresbury Laboratory, by molecular replacement using the program AMORE.

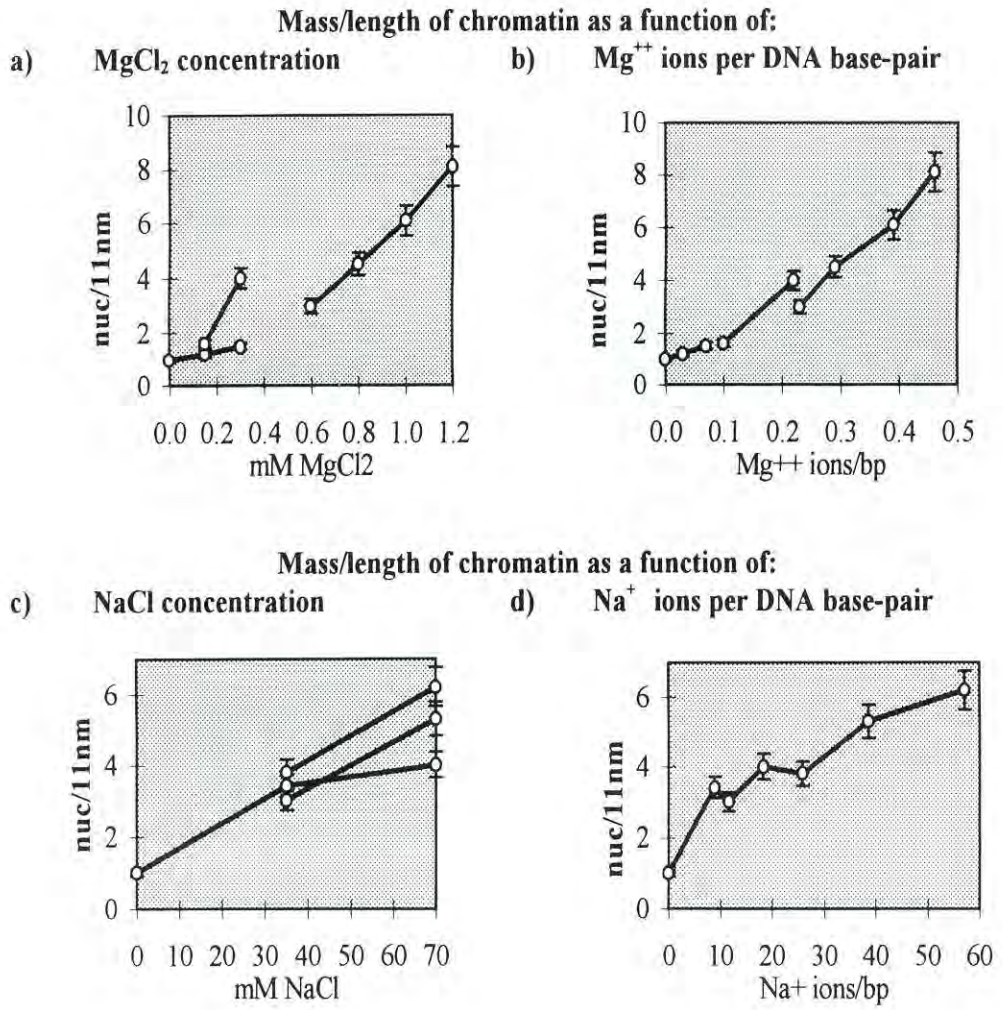

Figure 3: Comparison of the mass per unit lengths of multinucleosomes containing more than 100 nucleosomes and their dependence on the concentrations of Na^+ and Mg^{2+} ions from the same rod-Guinier plots used in Figure 2. These values were calculated from the intercepts of the ln(s.I(s)) vs s^2 plots on the ln(s.I(s)) axis. The data were put on an absolute scale by comparison with the scattering from standard solutions of nucleosome-core particles, so putting the mass per unit lengths in terms of nucleosomes per 11nm length. Note: 11nm comes from the literature on X-ray and neutron diffraction studies of chromatin fibres, where a meridional 11nm equivalent-spacing peak is observed.

Remarkably the crystal consists of left-handed helical arrays of histone octamers with six octamers per 10.2nm-c-axis repeat, which is strikingly similar to what would be the arrangement of histone octamers in the higher-order coil of nucleosomes discussed above. Questions arise therefore about whether the orientation of the octamers in the crystal has any relationship to the orientation of octamers in the coils of multinucleosomes and whether packing interactions between octamers in the crystals relate to interactions in the higher-order structure multinucleosomes in cell nuclei.

It has been suggested by Luger *et al.* [16], from the packing of nucleosome core particles in their $P2_12_12_1$ crystal structure, that the unit-cell packing interactions between basic amino-acid residues 16-25 of histone H4 and an acidic region on the surface of the H2A.H2B dimer may be important in the chromatin higher-order coil structure. This may be the case, of course, but the interactions between the histone-octamer molecules in the octamer crystals are of three types: 1) between residues 14 to 35 of histone H2A of one molecule and residues 24 to 53 of histone H4 of an adjacent octamer; 2) between residues 61 to 91 of histone H2A' of one molecule and residues 53 to 68 of histone H3' of an adjacent octamer; 3) between residues 105 to 120 of histone H2B' of one molecule and residues 21 to 36 of histone H4' of an adjacent octamer. Therefore it is not yet clear that protein-protein interactions between histone octamers directly occur in the higher-order structures of chromatin. The regions where interactions occur are shown on the map of the

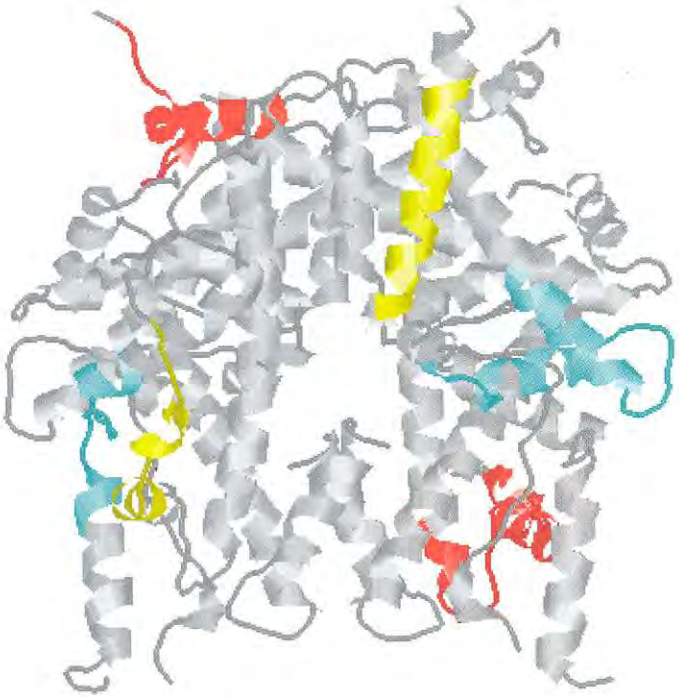

Figure 4: The structure of the histone octamer determined from the single crystal study at 2.15 Å resolution. The regions of interaction between octamers in the crystal structure are shown. Red: residues 14 to 35 of H2A of one molecule interact with residues 24 to 53 of H4 of an adjacent octamer. Blue: residues 61 to 91 of H2A' of one molecule interact with residues 53 to 68 of H3' of an adjacent octamer. Yellow: residues 105 to 120 of histone H2B' of one molecule interact with residues 21 to 36 of histone H4' of an adjacent octamer.

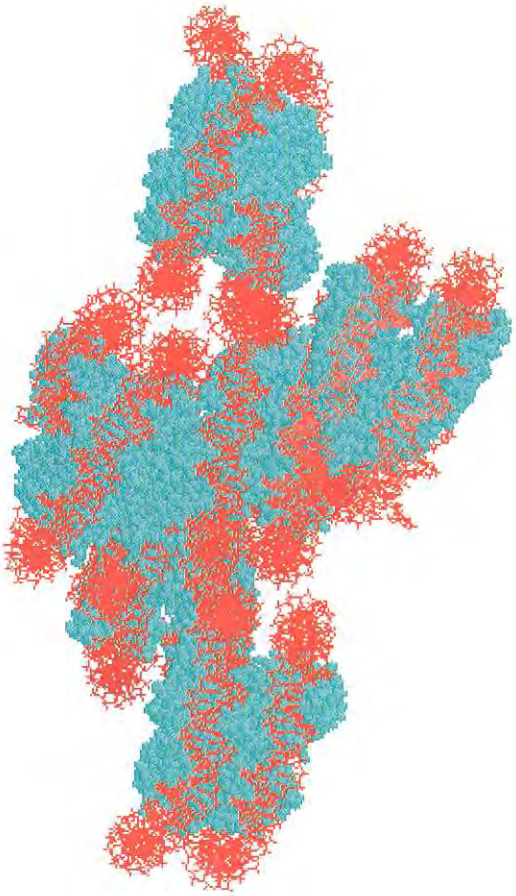

Figure 5: The packed arrays of octamers (blue) in the P65 crystal structure with the DNA (red) from the work of Luger *et al.* grafted on from their PDB file at the correct orientation to the octamers. The DNA fits onto the packed octamers without any clashes.

histone-octamer structure in Figure 4.

The packed arrays of octamers in the $P6_5$ structure are shown in Figure 5, with the DNA from the work of Luger *et al.* grafted on from their PDB file at the correct orientation to the octamers. Remarkably the DNA fits into the structure quite snugly.

Conclusions

Small-angle X-ray scattering studies of multinucleosomes, supported by photon-correlation and conductivity studies, show that Mg^{2+} ions fold the multinucleosomes in a different way from Na^{+} ions to form a more compact rod-like structure, dependent on the number of ions per nucleosome and not on the concentration of ions in the solution. Further the Mg^{2+} ions are "soaked up" by the multinucleosomes at very low ionic strength before the folding of them into a coiled structure commences. Histone octamers in the $P6_5$ crystal structure form helical arrays with parameters remarkably similar to what must be the arrays of octamers in the nucleosomes of chromatin higher structure. Inter-octamer interactions are not the same as in the nucleosome crystal structure, although they may be important in the multinucleosome–coils of chromatin higher-order structure.

Acknowledgements

We are grateful to Professor Colin Reynolds, Dr Fritjof Körber, Dr Amanda Reid, Mr Mike Donovan and Dr Dean Myles for many helpful discussions and support with X-ray facilities at Daresbury Laboratory. We thank Professor Hilary Evans for her encouragement and support from JMU. The work forms part of the Daresbury Laboratory Collaborative Research Program. The EPSRC of the UK gave support with a collaborative research grant.

References

[1] Graziano, V., Gerchman, S.E., Schneider, D.K. and Ramakrishnan, V., *Nature* (1994) **368**, 351-354.

[2] Lasters, I., Wyns, L., Muyldermans, S., Baldwin, J.P., Poland, G.A. and Nave, C., *Eur. J. Biochem.* (1985) **151**, 283-289.

[3] Williams, S.P., Athey, B.D., Muglia, L.J., Schappe, R.S., Gough, A.H. and Langmore J.P., *Biophys. J.* (1986) **49**, 233-248.

[4] Baldwin, J.P., Bosely, P.G., Bradbury, E.M. and Ibel, K., *Nature* (1975) **253**, 245-249.

[5] Widom, J. and Klug, A., *Cell* (1985) **43**, 207-213.

[6] Thoma, F., Koller, T. and Klug A., *J. Cell Biol.* (1979) **83**, 403-427.

[7] Staynov, D.Z., *Int. J. Biol. Macromol.* (1983) **5**, 3-9.

[8] Belikov, S. and Karpov, V., *Febs Lett.* (1998) **441**, 161-164.

[9] Allan, J., Hartman, P.G., Crane-Robinson, C. and Aviles, F.X., *Nature* (1980) **288**, 675-679.

[10] Lambert, S.J., Muyldermans, S., Baldwin, J., Kilner, J., Ibel, K. and Wins, L., *Biochem. Biophys. Res. Commun.* (1991) **179**,810-816.

[11]Baldwin, J.P., *Curr. Opin. Struct. Biol.* (1992) **2**, 78-83.

[12] Hayes, J.J. and Wolffe, A.P., *Proc. Natl. Acad. Sci. USA* (1993) **90**, 6415-6419.

[13] Kilner, J., Ph.D. Thesis (John Moores University 1993).

[14] Lambert, S.J., Nicholson, J.M., Chantalat, L., Reid, A.J., Donovan, M.J. and Baldwin, J.P. , *Acta Cryst. D* (1999) **55**, 1048-1051.

[15] Chantalat, L., Nicholson, J.M., Lambert, S.J., Reid, A.J., Donovan, M.J. and Baldwin, J.P., (submitted).

[16] Luger, K., Mader, A.W., Richmond, R.K., Sargent, D.F. and Richmond, T.J., Nature (1997) **389**, 251-260.

Real Time FTIR and WAXS Studies of the Drawing Behaviour of Polyethylene Terephthalate Fibres

A.C. Middleton[1], R.A. Duckett[1] and I.M. Ward[1], A. Mahendrasingam[2], C. Martin[2]

1 IRC in Polymer Science and Technology, University of Leeds, Leeds LS2 9JT.

2 Department of Physics, University of Keele, Keele ST5 5BG.

The development of molecular orientation and crystallisation has been studied during uniaxial drawing of polyethylene terephthalate (PET) films followed immediately by subsequent taut-annealing at the drawing temperature. The behaviour was monitored in real time throughout both drawing and annealing using dynamic FTIR spectroscopy and in situ WAXS measurements using the Daresbury Synchrotron Radiation Source.

The IR spectra were analysed using curve reconstruction procedures developed previously, and showed that orientation of the phenylene groups and the trans glycol conformers occurred before significant gauche-trans conformational changes could be seen. The onset of crystallisation, defined as the point that the crystalline $\bar{1}05$ reflection could be first observed using WAXS, was not found to correlate with any specific change in the proportions of trans and gauche isomers nor with any feature on the stress-strain curve. However, it was clear that for these comparatively low strain rates, crystallisation occurred during the drawing process, whilst the cross-head was moving, and the draw ratio was increasing.

Introduction

There is considerable evidence from studies of the solid phase deformation of polyethylene terephthalate and related polyesters to show that some aspects can be very well represented by the deformation of a molecular network. In particular, it appears that a molecular network is formed in melt spinning of fibres as the spun yarn cools in the threadline. Provided that no crystallisation occurs, the oriented spun yarn behaves like a frozen stretched rubber, so that a network draw ratio can be defined and quantitative stress-optical measurements can determine the molecular parameters of the network, such as the density of molecular

entanglements [1]. Further stretching, either by cold drawing below the glass transition temperature T_g, or hot drawing above T_g, involves further stretching of the molecular network. Where crystallisation occurs, the network draw ratio can be determined by curve matching *i.e.* fitting the strain hardening part of the room temperature true stress-true strain curves to the template for an isotropic unoriented spun yarn by a simple shift on the true strain axis (Figures 1(a) and 1(b)). It has been shown that properties such as modulus, tenacity and birefringence can then be related to the total network draw ratio [2] where the spin line stretch is added to the subsequent drawing stretch (Figures 2(a) and 2(b)).

Related structural measurements on the oriented PET have been undertaken by wide-angle and small angle X-ray diffraction and by a range of spectroscopic

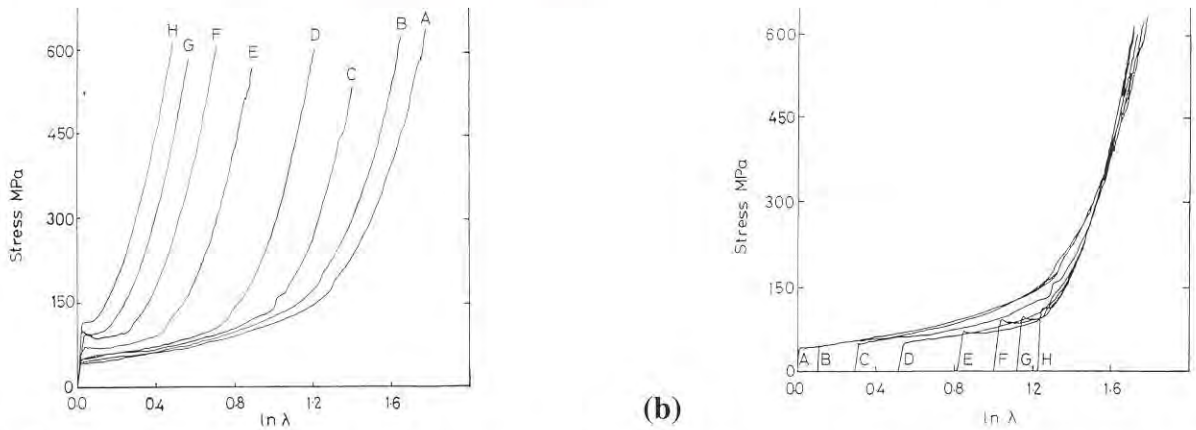

Figure 1: (a) True stress-strain curves for spun yarns. A to H is increasing spun yarn orientation. (b) Matching of true stress-strain curves for spun yarns.

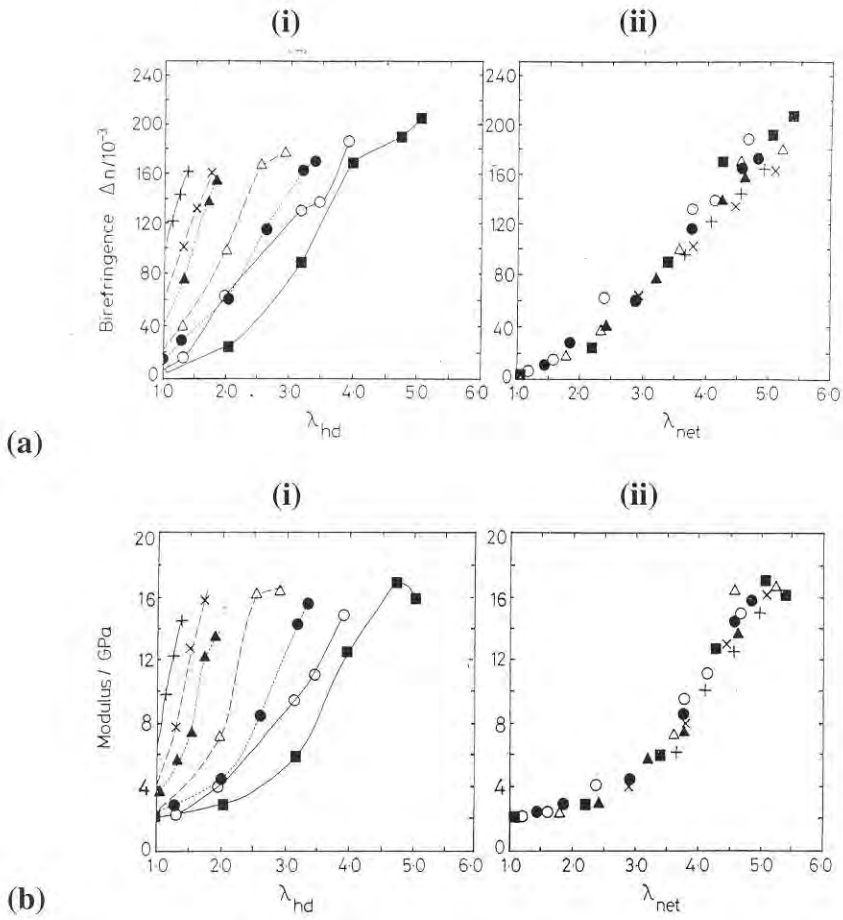

Figure 2: (a) Birefringence vs actual hot draw ratio λ_{hd} (i) and network draw ratio λ_{net} (ii) for spin-drawn yarns and their spun yarn precursors. (b) Initial modulus vs actual hot draw ratio λ_{hd} (i) and network draw ratio λ_{net} (ii) for spin-drawn yarns and their precursors. A = squares, B = hollow circles, C = filled circles, D = hollow triangles, E = filled triangles, F = diagonal crosses, H = crosses, where A to H is increasing spun yarn orientation due to increased wind-up speed)

techniques, including infra-red, Raman and polarised fluorescence spectroscopy and NMR. For high wind-up speed fibres for drawing above T_g with draw ratios greater than about 2.5, crystallisation occurs. At a molecular level the chain conformations which are primarily crumpled *gauche* conformations in the isotropic polymer are transformed into extended *trans* conformations, which exist in the crystalline regions as shown by the crystal structure determined by Bunn and co-workers [3]. The development of molecular orientation and the changes in *trans/gauche* content have also been very successfully modelled by the deformation of a molecular network (Figures 3(a) and 3(b)) [4].

It is remarkable that the correlations between properties and network draw ratio and the simple algorithms developed for the development of molecular orientation and conformational changes appear to be insensitive to the onset of crystallisation. This observation has led to the research described in this article where wide-angle X-ray diffraction measurements made *in situ* during the drawing process are combined with FTIR Raman measurements also made in-line to monitor molecular orientation and *trans/gauche* content.

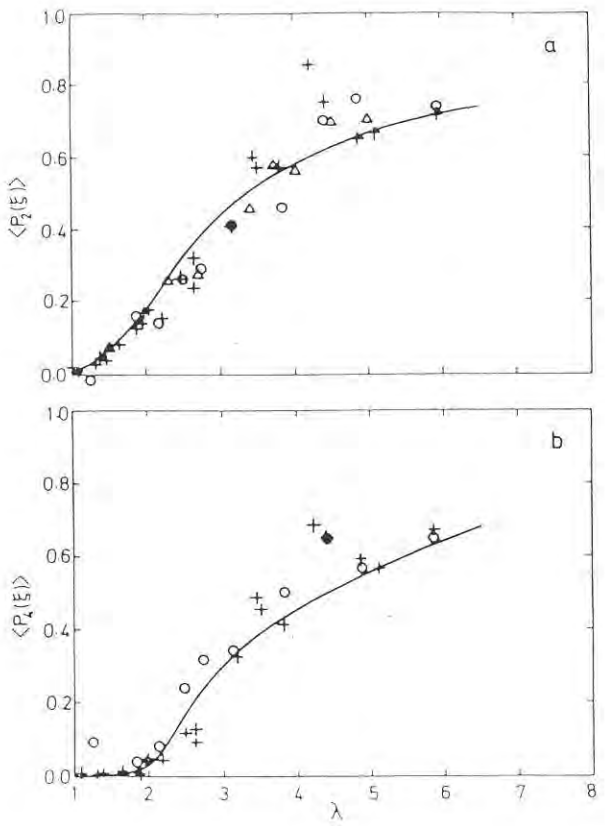

Figure 3: Development of molecular orientation as a function of draw ratio. $\langle P_2(\xi)\rangle$ and $\langle P_4(\xi)\rangle$ are the second and fourth Legendre functions describing molecular orientation. Theoretical predictions = solid line, experimental results from refractive index measurements = triangles, fluorescence measurements = crosses, Raman measurements = circles.

Experimental

I-R spectroscopy

Polarised I-R spectra were recorded in real-time by drawing samples in a Minimat materials tester mounted on the sample stage of a BOMEM MB-151 FTIR spectrometer. The spectrometer was controlled by a NEC personal computer using commercially available Spectra-Calc software. The chamber was heated by the circulation of hot air and the glass entry and exit windows were replaced with potassium bromide (KBr). Parallel and perpendicular polarisation spectra were recorded on successive samples which underwent identical thermal and mechanical histories. This could be justified because drawing under these conditions was found to be almost perfectly reproducible. A schematic of the Minimat showing the experimental arrangement required for the collection of polarised spectra whilst the sample is both heated and drawn is shown in Figure 4.

WAXS

The samples studied using WAXS were drawn in a purpose built X-ray camera [5,6]. The camera was heated by two heating elements and the air was circulated by wall mounted fans. The camera was mounted on its side and positioned so that the sample was tilted through an angle of 21° towards the

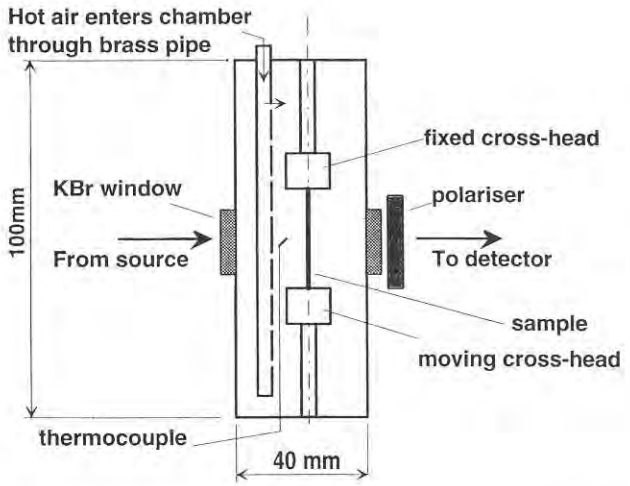

Figure 4: Schematic diagram of temperature chamber for the Minimat material tester mounted on the BOMEM sample stage.

incident beam. The instrumentation required to perform dynamic experiments and collect diffraction patterns in real-time using the Keele camera is discussed fully in [7].

All the real-time WAXS experiments were carried out at the Daresbury SRS. The beam had a monochromated wavelength of 1.488Å and the current varied from 156 mA to 131 mA during each 24 hour period. The diffraction patterns were collected using a CCD camera. The camera was placed normal to the incident X-ray beam and close to the aluminium foil window in order to minimise air scatter. Unfortunately the size of the detector area and the geometry of the experiment meant that only part of the pattern was recorded. The detector was therefore carefully positioned so that it was able to record both the centre of the diffraction pattern and the $\bar{1}05$ reflection.

Results and Discussion

I-R Spectroscopy

Figures 5(a) and 5(b) show the variation in the *trans* and *gauche* conformer contents and the orientation of the *trans*, *gauche* and benzene ring bands respectively for samples drawn at 80°C and at a cross-head speed of 5mm/min.

The majority of the *gauche* to *trans* conversion occurred whilst the cross-head was moving, but there were also some changes during the annealing period whilst the draw ratio remained constant. It should be noted that the possible variations in the conformer contents at the final draw ratio appear artificially high on these graphs since random scatter in the data will have the same appearance as a genuine trend when all the data points are plotted at the same draw ratio. There do not seem to be any sudden changes in the *trans/gauche* ratio which could relate to the onset of crystallisation.

WAXS

The progression of the crystallisation of each sample was monitored by recording the peak intensity of the reflection and comparing it with the draw ratio at that time. The crystallinity is actually related to the integrated area under the reflection, but, since the Gaussian half width of the reflection underwent very little change during the course of each experiment, a semi-quantitative study can be completed by considering simply the peak intensity. Figure 6 shows the development of the crystalline $\bar{1}05$ peak for samples drawn at 5mm/min.

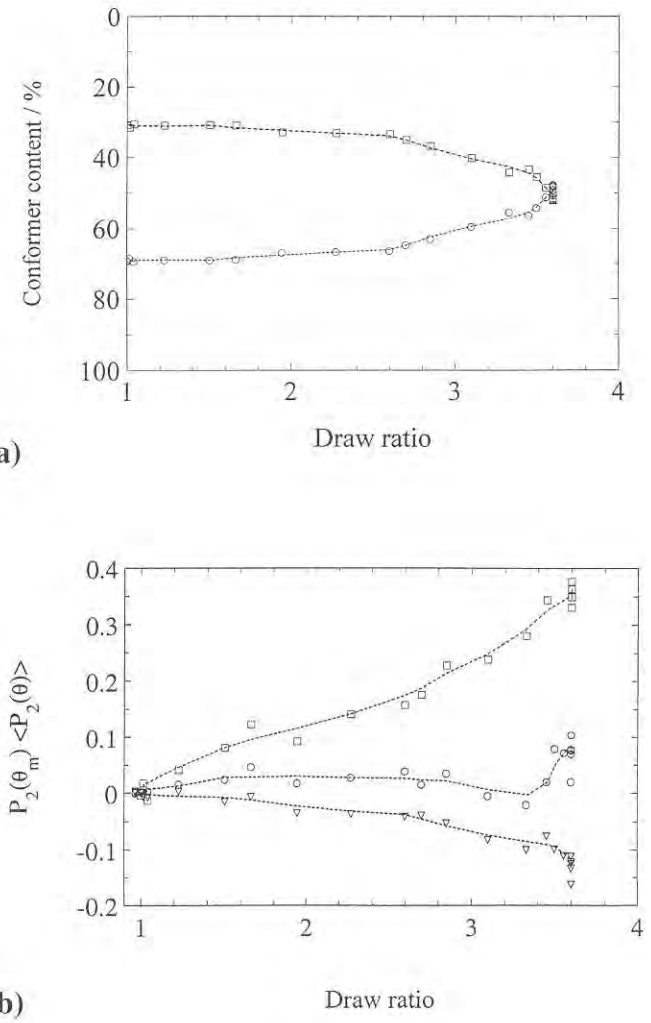

Figure 5: (a) *Trans* (squares) and *gauche* (circles) contents as functions of draw ratio for sample drawn at 80°C and cross-head speed 5mm/min. (b): Orientation of 972cm^{-1} *trans* (squares), 890 + 899 + 906 cm^{-1} *gauche* (circles) and 872 + 878 cm^{-1} benzene ring band (triangles) as a function of draw ratio for sample drawn at 80°C and 5mm/min.

Crystallisation clearly occurs during the draw. Once it has reached a recordable level, the peak intensity of the azimuthal scan then increases approximately linearly throughout the remainder of the draw. It may be that the development of the crystalline reflection proceeds smoothly from zero in which case the peak may have existed in earlier diffraction patterns without rising clear of the noise. Alternatively the peak behaviour may be as presented here such that the peak initially shows discontinuous growth. This would agree with the hypothesis of other researchers that crystallisation is initiated from many different centres as soon as a critical condition is established

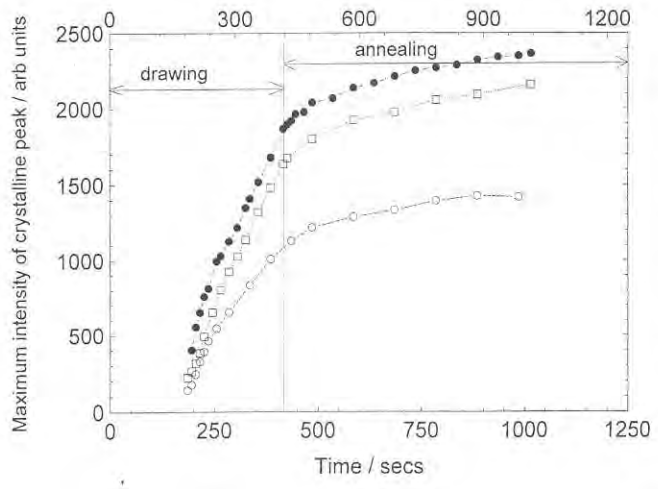

Figure 6: Development of crystalline peak during drawing and annealing of samples drawn at 5mm/min. 85°C thick = hollow circles, 80°C thin = filled circles, 80°C thick = squares.

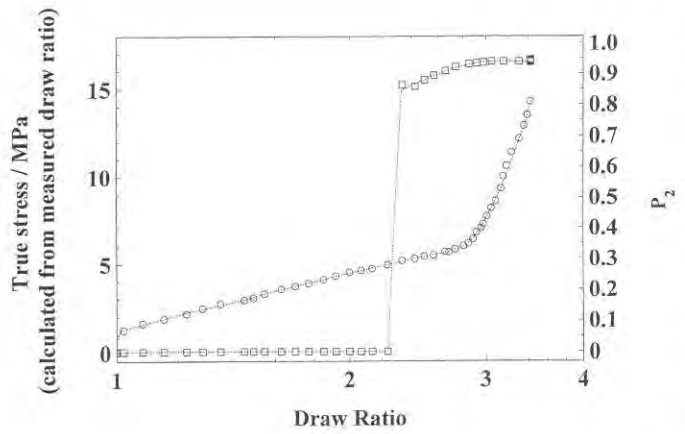

Figure 7: P_2 (squares) and true stress (circles) versus draw ratio for thick samples drawn at 80°C, 5mm/min.

(*e.g.* the amorphous orientation passes a certain level) [8,9]. Draw ratios at which the reflection first became apparent during each experiment were always close to 2.5 and it was difficult to discern any other trend from the data.

Figure 7 shows the variation of the orientation parameter $\langle P2(q) \rangle_{\bar{1}05,m}$ and the true stress values with draw ratio for the 200μm sample drawn at 80°C and 5mm/min. The orientation parameter has been abbreviated to P_2 in the figure. The point at which a Gaussian curve can first be fitted to the WAXS data does not seem to correspond to any particular feature on the true stress-strain curve and the majority of the draws under all conditions showed a similar lack of correlation between the onset of crystallisation and the true stress *vs* strain. The orientation of the $\bar{1}05$ crystallites is always very high, appearing with values of 0.80 to 0.90 and rising to 0.95 by the end of the annealing period, regardless of the drawing conditions.

The most significant conclusion which can be drawn from the real-time WAXS results is that the crystallisation occurs whilst the cross-head is moving and the draw ratio is increasing. This is further confirmation of recent results by Blundell *et al.* [7]. The crystalline peak was first observed for draw ratios close to 2.5 and no clear trend emerged from the data between the draw ratio and the temperature or speed of drawing. However, the fraction of the final intensity which developed whilst the cross-head was moving showed a definite correlation with the drawing speed and implied that drawing at very high speeds would result in crystalline reflections which developed entirely after the cross-head stopped moving.

Conclusions

The combination of FTIR spectroscopy and WAXS results taken during the drawing and taut annealing of PET film has provided considerable insight into the mechanism of drawing and crystallisation. *Gauche/trans* isomerisation is clearly detectable during drawing, at a rate which increases with increasing draw-rate and decreasing temperature. The orientation of the *trans* conformers also increased in a similar way. The WAXS technique is sensitive only to those *trans* conformers in crystalline regions and these are only detected at draw-ratios above approximately 2.2. When observed, the crystallites are seen to be highly oriented – more oriented than the overall *trans* orientation. The onset of crystallisation as detected by WAXS is not marked by any sudden change in number or orientation of *trans* conformers, nor with any particular feature of the stress-strain curves. There is clear evidence that crystallisation is occurring during the drawing process, although at the higher drawing speeds the majority of the crystallisation observed occurred during the taut-annealing process.

Acknowledgements

A. C. Middleton held an EPSRC CASE studentship sponsored by ICI Films. The authors thank Dr D. J. Blundell and Dr D. MacKerron of ICI Films for their contributions to this research.

References

[1] Pinnock, P.R. and Ward, I.M., *Trans. Faraday Soc.* (1966) **62**, 1308.
[2] Long, S.D. and Ward, I.M., *J. Polym. Sci. Polym. Phys. Ed.* (1991) **42**, 1921.
[3] Bunn, C.W., Daubeny, R. de P. and Brown, C.J., *Proc. Roy. Soc. A* (1954) **10**, 275.
[4] Nobbs, J.H., Bower, D.I. and Ward, I.M., *J. Polym. Sci. Polym. Phys. Edn* (1979) **17**, 259.
[5] Mahendrasingam, A., MacKerron, D.H., Fuller, W., Forsyth, V.T., Oldman, R.J. and Blundell, D.J., *Rev. Sci. Instrum.* (1992) **63**, 1097.
[6] Blundell, D.J., Mahendrasingam, A., MacKerron, D.H., Turner, A., Rule, R., Oldman, R.J. and Fuller, W., *Polymer* (1994) **35**, 3875.
[7] Blundell, D.J., MacKerron, D.H., Fuller, W., Mahendrasingam, A., Martin, C., Oldman, R.J., Rule, R. and Riekel, C., *Polymer* (1996) **37**, 3303.
[8] Salem, D.R., Polymer (1992) **33**, 3189.
[9] Salem, D.R., Polymer (1992) **33**, 3182.

8th Annual Workshop Prize-Winning Posters

An XRD Study of the Rigid-Rod Polymer Fibre M5 (PIPD)

E.A. Klop and M. Lammers

Akzo Nobel Central Research, P.O.Box 9300, 6800 SB Arnhem, Netherlands.

Introduction

The spinning of rod-like polymer molecules from liquid crystalline solutions has proven to be an effective way of preparing fibres that exhibit high stiffness and tenacity. The high level of molecular orientation already present in the as-spun state can be further increased by heat treatment resulting in materials suitable for high-performance structural applications. This spinning and heat treatment process is used in the production of the rigid-rod polymer fibre poly (*p*-phenylene benzobisoxazole) (PBO). The performance of this fibre (and related fibres) in compression, however, is disappointing, due to the absence of strong interchain bonding. In recent years much effort has been spent on increasing the lateral strength of rigid rod polymer fibres, often by crosslinking after fibre formation. These efforts were not very successful.

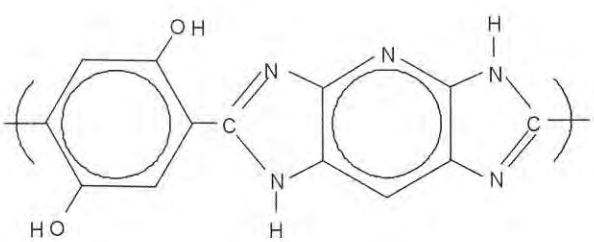

Figure 1: Chemical structure of M5.

Figure 1 shows the structural formula of the rigid-rod polymer M5, which was discovered in our laboratory [1]. The design of this polymer, with chemical name poly{2,6-diimidazo[4,5-b:4'5'-e]pyridinylene-1,4(2,5-dihydroxy) phenylene}, abbreviated as "PIPD", was motivated by its ability to form intermolecular hydrogen bonds. Fibres spun from a nematic solution of the polymer in polyphosphoric acid not only exhibit a high stiffness and tenacity (330 and 5 GPa respectively), but also a compression strength (1.7 GPa) which exceeds that of any other polymer fibre. Compared with carbon fibre, the material has the advantage of having a very high damage tolerance; moreover, it is an electrical insulator. While the heat-treated material has attractive properties, the as-spun material is interesting as well, as it is highly fire-resistant. The work reported here concerns the structural order both in heat-treated and as-spun M5 fibre.

Heat-treated M5 fibre

The diffraction pattern of heat-treated M5 fibre (Figure 2(a)) shows several reflections on the first three layer-lines, indicating three-dimensional crystalline order. Despite the small number of reflections, it was possible to determine the unit cell parameters and the packing of the polymer molecules, using a diffraction modelling approach. Based on the flat plate diffraction pattern, two models are proposed which have the same lattice (with parameters 12.60 Å, 3.48 Å, 12.01 Å, 90.0°, 108.6°, 90.0°) but different symmetry, *viz.* a triclinic

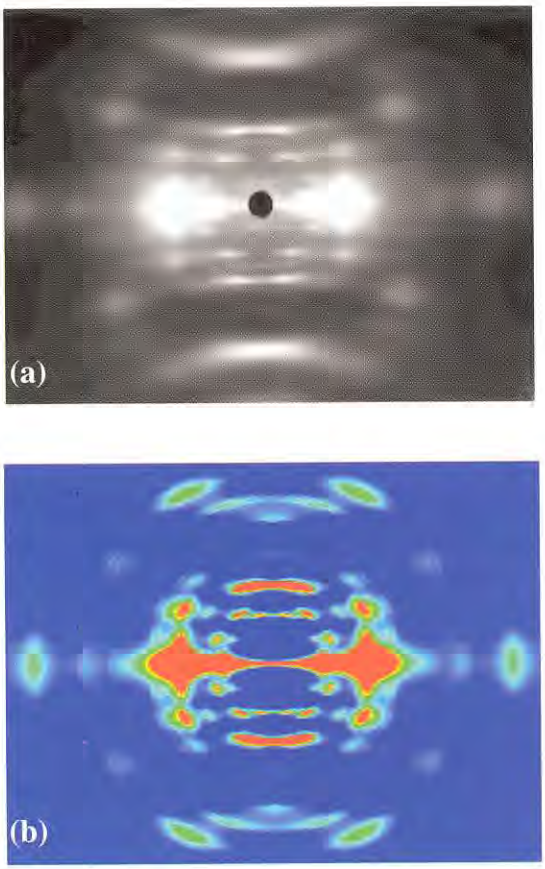

Figure 2: Flat plate diffraction pattern of heat-treated M5 fibre, (a) observed, (b) calculated (based on the monoclinic model).

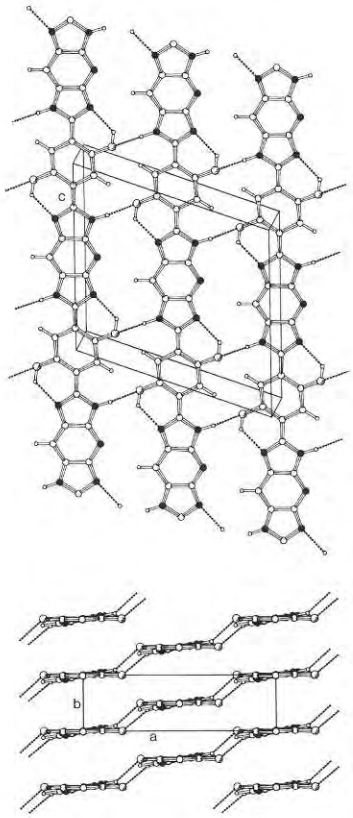

Figure 3: Triclinic model of heat-treated M5 fibre with sheet-like hydrogen bonding scheme. The upper picture shows the polymer chains at the (x, y) positions (0, 0), (1/2, 1/2) and (1, 1). Nitrogen atoms are coloured black, oxygen atoms are drawn somewhat larger to discriminate them from carbon atoms.

model (described for obvious reasons in a *c*-centred unit cell, see Figure 3) and a monoclinic model with *Pa* symmetry (pseudo $P2_1/a$) (Figure 4). The key interchain interaction in these models is N-H—-O hydrogen bonding. The only difference between the models is that in the monoclinic model the heterocyclic fragment of the centre chain is rotated in the opposite direction compared to that of the corner chain, unlike in the triclinic model. This influences the hydrogen bonding scheme drastically: the triclinic model exhibits a sheet-like hydrogen bonding scheme, whereas in the monoclinic model the intermolecular hydrogen bonds form a bi-directional hydrogen bonding network. Figure 2(b) shows the diffraction pattern calculated on the basis of the monoclinic model. Due to the limited crystalline perfection it is impossible to discriminate between the two models on the basis of the flat plate diffraction pattern. However, as the two models differ in the intermolecular interactions along the diagonals of the unit cell, useful information can be obtained from thermal expansion data as provided by high-temperature XRD. For the sheet-like model one would expect different coefficients of thermal expansion for the (1 1 0) and (1 –1 0) planes, *i.e.* a

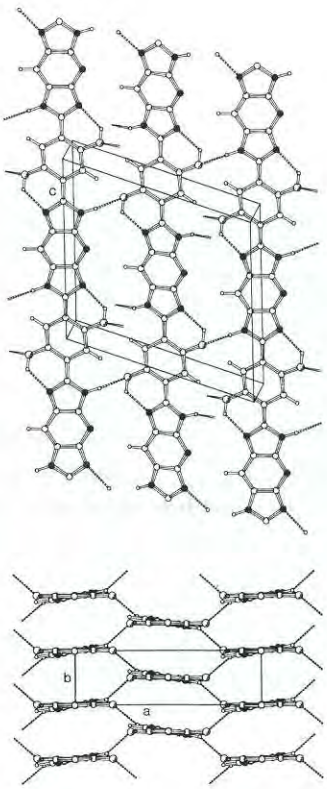

Figure 4: Monoclinic model of heat-treated M5 fibre with bi-directional hydrogen bonding network. The only difference with the model in Figure 3 is that the *c*-centering is replaced by *a*-glide symmetry.

splitting up of the corresponding 3.34 Å peak (2q = 26.7°) in the equatorial diffraction pattern with temperature. As such splitting up is not observed, it can be concluded that the coefficients of thermal expansion for the two planes are equal, which is consistent with the monoclinic model. We therefore conclude that the crystal structure of heat-treated M5 fibre is monoclinic, although it may exhibit sheet-like distortions. The bi-directional hydrogen bonding scheme implied by the monoclinic symmetry leads to a honeycomb structure which provides a satisfactory explanation for the good compression performance of the material.

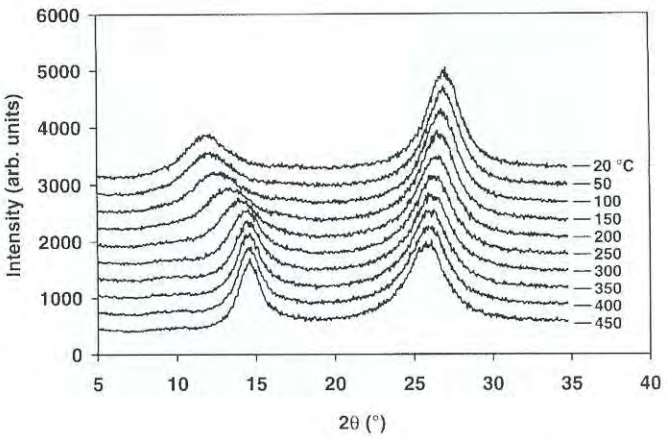

Figure 5: Equatorial X-ray scattering of as-spun M5 fibre as function of temperature in a nitrogen atmosphere. The first peak is the 2 0 0 peak, the second peak is indexed as 1 1 0 and 1 –1 0.

As-spun M5 fibre

Surprisingly, the structure of the as-spun fibre differs completely from that of the heat-treated material, quite unlike other rigid-rod fibres where heat treatment merely leads to increased crystalline perfection. The material lacks three-dimensional crystalline order due to translational disorder of the polymer molecules in the direction of the fibre axis. The polymer chains pack in a two-dimensional lattice described by a non-primitive rectangular unit cell with parameters a = 16.85 Å, b = 3.38 Å. The a-axis is much larger than that in the heat-treated material, which is due to the presence of water molecules in the crystal lattice: the as-spun material is a hydrate in which stacks of polymer molecules are separated by sheets of hydrogen bonded water molecules. Heat treatment (or flushing with dry nitrogen) causes dehydration of the material. This is accompanied by a shift of the 2 0 0 reflection to larger diffraction angles, as can be observed in Figure 5 which shows the changes in the equatorial X-ray scattering of as-spun M5 upon heating. The *continuous* shift of this reflection indicates that in partly dehydrated material the two-dimensional lattice is disordered in the direction of the a-axis. This disorder can be described by a model assuming a random distribution of two repeat units in the a direction [4], as is shown schematically in Figure 6. Hence we propose that partly dehydrated M5

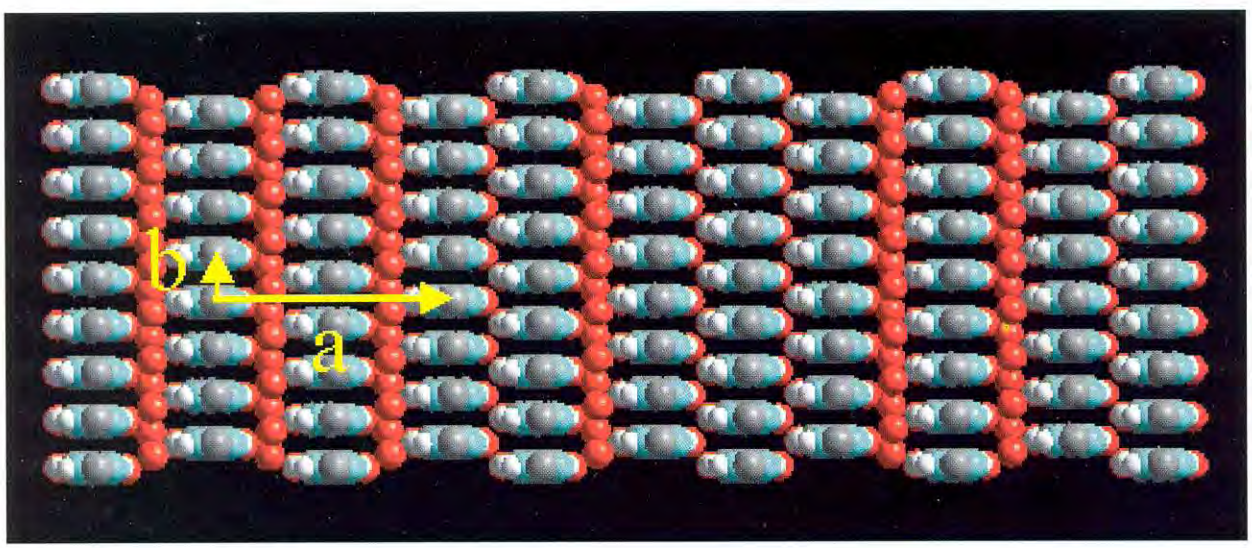

Figure 6: Schematic model of partially (de)hydrated M5 fibre showing lattice disorder in the a direction. The a and b-axes of as-spun M5 fibre are indicated in yellow. Oxygen, nitrogen and carbon atoms are coloured red, blue and grey respectively. The hydrogen atoms of the water molecules have been omitted. Note that in the illustration neighbouring stacks of polymer molecules are assumed to be correlated in the b direction. However, the stacks of polymer molecules which are separated by a sheet of water molecules may show translational disorder in the b direction. Such disorder may also exist in as-spun M5 fibre (*i.e.* in completely hydrated material).

consists of crystallites in which stacks of polymer molecules and sheets of water molecules form a non-periodic sequence. A related type of disorder is found in completely different material, *viz.* in random copolymers of two types of monomers that differ in molecular length [5, 6]. Crystallites based on identical but non-periodic sequences within neighbouring copolymer molecules were designated NPL (non-periodic layer) crystallites by Windle *et al.* [6]. Generalizing the concept of NPL crystallites somewhat, the crystallites in partly dehydrated M5 can also be referred to as NPL crystallites. Clearly, the hydrogen bonded water molecules in as-spun M5 contribute to the high fire resistance of the material. The model in Figure 6 suggests that dehydration proceeds via a "zipper" mechanism, so that removal of water molecules from a sheet that has already lost some water molecules has a higher probability than removal of water molecules from an entirely intact sheet of water molecules.

Acknowledgements

This work would have been impossible without the unflagging zeal of Dr Doetze Sikkema in making the M5 project successful. The authors also wish to acknowledge the stimulating interest of Dr. Maurits Northolt and a helpful discussion with Prof. Alan Windle.

References

[1] Sikkema, D.J., *Polymer* (1998) **39**, 5981-5986.

[2] Klop, E.A. and Lammers, M., *Polymer* (1998) **39**, 5987-5998.

[3] Lammers, M., Klop, E.A., Northolt, M.G. and Sikkema, D.J., *Polymer* (1998) **39**, 5999-6005.

[4] "b direction" should be replaced by "a direction" in ref. [2], p. 5996.

[5] Blackwell, J., Biswas, A. and Bonart, C., *Macromolecules* (1985) **18**, 2126-2130.

[6] Windle, A.H., Viney, C., Golombok, R., Donald, A.M. and Mitchell, G.R., *Faraday Disc. Chem. Soc.* (1985) **79**, 55.

X-Ray Analysis of the Network-Forming Collagen in the Dogfish Scyliorhinus Canicula Egg Case

C. Knupp and J.M. Squire

Biological Structure and Function Section, Biomedical Sciences Division, Imperial College School of Medicine, London SW7 2AZ.

Introduction

Network-forming collagens are essential to life for most multicellular organisms. In basal membranes, which are the part of the extracellular matrix that remain in direct contact with their formative cells, they accomplish supportive, protective and filtering roles, and they help cellular attachment, differentiation, migration and growth [1]. In human eyes, the building of abnormal collagen-like networks is related to serious sight threatening diseases that are poorly understood. Of these, age related macular disease alone is responsible for about 50% of the cases of legal blindness in the western world [2]. Structural studies of these molecular organisations are the first step towards understanding their function in the structures that they form or in the pathologies with which they are associated. Unfortunately, in most cases, network-forming collagens assemble into structures that are poorly ordered, making structural investigations particularly difficult. One way round this problem is to find and study in detail a network-forming collagen that assembles naturally in a regular way, in the hope that it can give general insights into the way network-forming collagens behave. The egg case of the dogfish *Scyliorhinus canicula* appears to be a very appropriate candidate for this task. It is formed by a collagen network that naturally possesses a high degree of order. Like the basal membrane it fulfils a supportive, protective and filtering role, being the only medium between the embryo and the sea. Furthermore, its molecular arrangement is strikingly similar to that found in the ocular assemblies associated with age related macular disease.

Dogfish Egg Case

With the naked eye, the capsule containing the dogfish egg appears as a small convex rectangular-shaped container, 50 by 20 mm on average (Figure 1). The two anterior and the two posterior corners are elongated to form horn-like structures that continue their extension as four long, coiled, thread-like

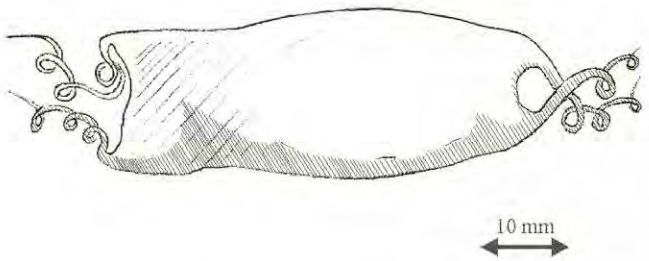

Figure 1: Schematic drawing of the dogfish *Scyliorhinus canicula* egg case. The capsule is about 50 mm x 20 mm and its corners are elongated into four tendrils that attach to seaweeds when the eggs are laid.

filaments, generally referred to as tendrils. These tendrils are used by the females to attach the newly laid eggs to any available supports such as seaweeds or stones. Unlike avian or reptilian egg cases, fish egg cases do not have to prevent water losses, but they still have to allow gaseous exchange for respiration. The dogfish egg case wall has been shown to be highly permeable to small ions and small molecular weight polar solutes, with diffusion channels showing an estimated pore radius of 1.36 nm [3].

Evidence for the collagenous nature of the dogfish egg case [4,5,6] was obtained from X-ray diffraction studies (that indicated the existence of a 0.29 nm meridional arc), thermal shrinkage studies (which produced a thermal shrinkage curve typical for collagen that was S-shaped and with a mean half shrinkage temperature of 78°C) and amino acid analysis (which showed that glycine accounted for about 16% of all amino acid residues with repeated Gly-X-Y regions in the amino acid sequence). The dogfish egg case collagen was purified and observed in the electron microscope after metal shadowing. It appears to be about 40 nm long with a large globular domain at one end (about 4 nm in diameter) and a much smaller one at the other end [7].

The egg case wall is approximately 2 mm thick when wet. It is mainly composed of laminae (about 0.5 μm thick) that become progressively thicker towards the inner surface of the egg case [8,9,7]. In longitudinal sections, the laminae that form the bulk of the thickness of the egg case show a regular alternation of density. Successive laminae show low, intermediate, high, intermediate and low densities and this pattern repeats, more or less regularly through nearly the whole thickness of the egg case. When the laminae are examined at high magnification, the dense ones are seen to contain fibrils sectioned longitudinally, while all the fibrils in the light laminae have been sectioned transversely (Figure 2). The laminae of intermediate density show obliquely sectioned fibrils running parallel to the surface of the egg case. This appearance suggested an orthogonal construction similar to that of plywood in which successive laminae are made up from sheets of parallel fibres [7].

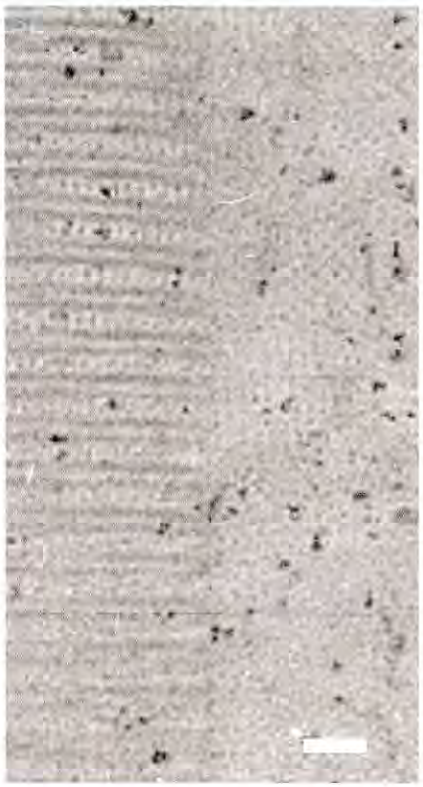

Figure 2: Electron micrograph of the egg case showing two abutting laminae with different fibril orientations. Bar 50 nm.

The fibrils within the laminae appear rather closely packed and show a paracrystalline construction. In transverse section the paracrystalline lattice appears coherent over roughly circular areas up to 150 nm which probably represent the width of the whole fibril. The fibrils present a body-centred square lattice of ordered dots of 10 nm side (Figure 3(a)). In longitudinal sections, pairs of bands of protein density about 13 nm apart can be seen to repeat every 40 nm, with filaments of protein density running axially between the bands (Figure 3(b)). The molecular arrangement within the unit cells was studied using transmission electron microscopy and was found to belong to the *I*422 space group with dimensions of about 10 by 10 by 80 nm [10]. A three-dimensional reconstruction was obtained by combining electron microscope data from different views through the unit cell (Figure 4). A model that fitted the reconstruction was proposed [11] in which

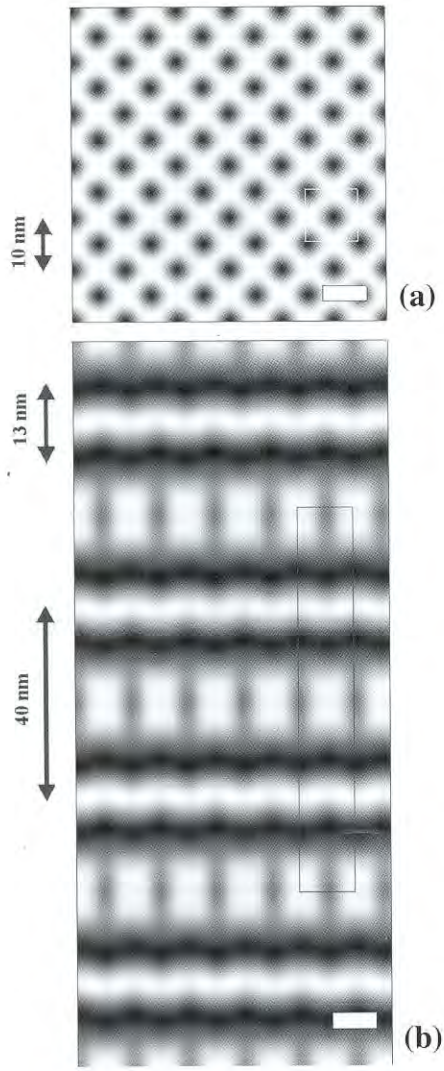

Figure 3: (a) Two-dimensional Fourier synthesis of a transverse appearance of the molecular arrangement in the dogfish egg case. The two-dimensional body-centred unit cell of dimensions about 10 X 10 nm is highlighted in white. (b) Fourier synthesis of a longitudinal appearance. Pairs of bands 13 nm apart are seen running laterally with a 40-nm axial periodicity. Axially, filaments of protein density run through the bands. Proteins are shown in dark tones. Bars 10 nm.

sixteen 40-nm-long collagen molecules occupy each unit cell, with every molecule connected at each terminus to another molecule in a head-to-tail arrangement (Figure 5).

X-Ray Diffraction Studies [12]

Before the X-ray study, pieces of *Scyliorhinus canicula* dogfish egg case wall were removed and washed in distilled water. Successively, laminae were stripped off these and cut into small strips a few hundred microns thick to fit glass capillaries 0.5 mm in diameter. The capillaries were then exposed to the X-ray beam in the beam line 2.1 at the Daresbury synchrotron. The camera was set up with a 2.5 m

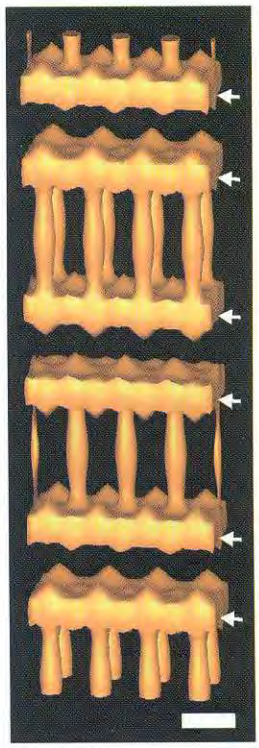

Figure 4: Three-dimensional reconstruction of the molecular arrangement in the fibrils that form the egg case laminae. Arrows highlight the features coming from the lateral pairs of bands seen in Figure 3(b). Axial 'pillars of protein density run between the pairs of bands. Bar 10 nm.

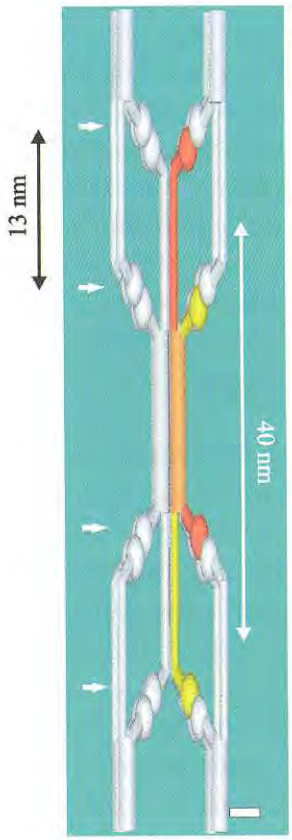

Figure 5: Proposed molecular arrangement within the dogfish egg case unit cell. Sixteen molecules occupy each unit cell. In red and yellow are highlighted two molecules that interact laterally to give rise to the orange filament seen in the figure. Four such filaments associate laterally to give rise to the axial filaments of protein density of Figure 3, or to the axial 'pillars' of the reconstruction in Figure 4. The arrows show the position of the lateral bands (see Figure 3(b) and 4). Bar 3 nm.

long vacuum tube and patterns were collected on an area detector. The acquisition time could vary from a few seconds to 5 minutes. During this time the specimens were kept at 100% humidity by means of a water reservoir in the capillaries. X-ray diffraction patterns of the wall were taken along mutually perpendicular directions, one being perpendicular to the surface of the egg case. Three kinds of diffraction pattern were recorded as shown in Figure 6. One pattern was characteristic of an X-ray direction perpendicular to the laminae in the egg case (Figure 6(a)). Another pattern was observed in either of the two directions parallel to the laminae (Figure 6(b)). A third pattern was observed with the X-rays almost parallel to the plane of the laminae (Figure 6(c)).

The X-ray diffraction pattern obtained with the X-ray beam perpendicular to the laminae (Figure 6(a)), shows rings of intensity corresponding to an 80 nm repeat (arrowheads). In one of the observed patterns with the X-rays parallel to the laminae (Figure 6(b)) even orders of an 80 nm repeat (arrowheads) are present along the meridian. On the equator there is a strong reflection corresponding to a 7 nm spacing (chevron) and on the first layer-line there are two reflections corresponding to a 10 nm spacing (arrows). The 10 nm reflections are connected by an arc which occurs everywhere except on the equator. The 7 nm reflection also smears into arcs. In the pattern taken with the X-rays almost parallel to the laminae (Figure 6(c)), reflections corresponding to an 80 nm repeat are observed on the meridian (arrowheads). On and close to the equator there are three reflections corresponding to 10 nm which prolong to form a circle.

In order to interpret the diffraction pattern, a Fourier space model of the fibrils was built (Figure 7(a)). The superposition of several of these models, corresponding to different fibre directions, gives rise to a model in Fourier space. This, in turn, if correct must explain the diffraction patterns recorded experimentally once the nature of the intersection with the Ewald sphere has been included (Figure 7(b)). The Fourier space model included a series of 80 nm repeat reflections on the fibril axis and rings corresponding to 10 nm and 7 nm spacings. The existence and position of the features included in the model were inferred from the Fourier transform of the electron micrographs of the egg case [10]. Figure 8 illustrates, as an example, the origin of the diffraction pattern in Figure 6(b). Fibres that are 15° apart and with a horizontal 'average' direction (see

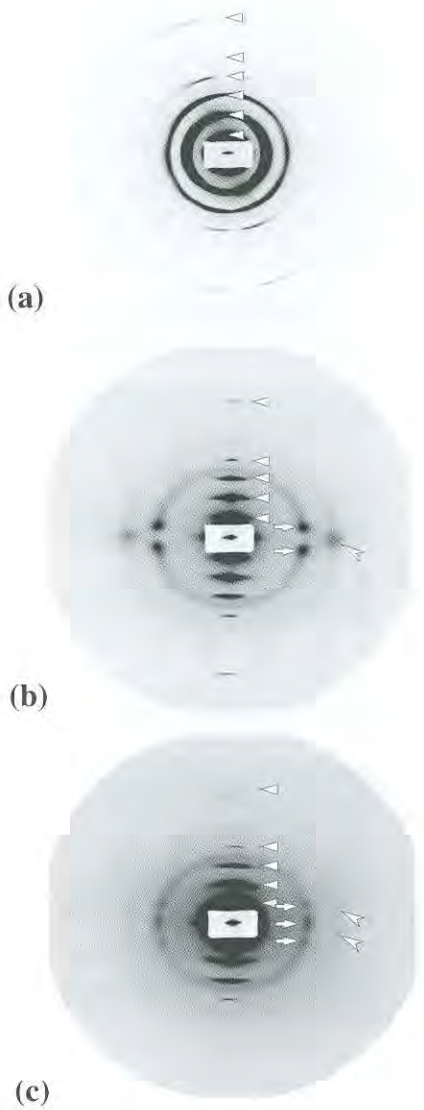

Figure 6: (a) Low- angle diffraction pattern from the dogfish egg case wall obtained with the X-ray beam perpendicular to the laminae in the egg case. Rings of intensity corresponding to orders of a 80 nm repeat are seen (arrowheads). (b) Diffraction pattern with the X-ray beam along a direction parallel to the laminae. On the meridian are even orders of an 80-nm repeat (arrowheads). On the equator there is a strong reflection corresponding to a 7 nm spacing (chevron). The first layer line has reflections corresponding to a 10-nm spacing (arrows). (c) Alternative X-ray diffraction pattern to (b), obtained with the X-ray beam along a direction almost parallel to the laminae in the egg case wall. Reflections corresponding to even orders of an 80-nm repeat are observed on the meridian (arrowheads). On the equator and on a layer-line, it is possible to observe three reflections corresponding to a roughly 10 nm spacing, which lie on a complete circle of intensity. The chevrons highlight two weak reflections corresponding to about 7 nm.

Figure 8(a)) generate the pattern in Figure 8(b) when they intersect the Ewald sphere (a portion of which is drawn in red in Figure 8(a). Fibres oriented vertically (see Figure 8(c)) give the pattern in Figure 8(d). If both main fibre directions are present in the

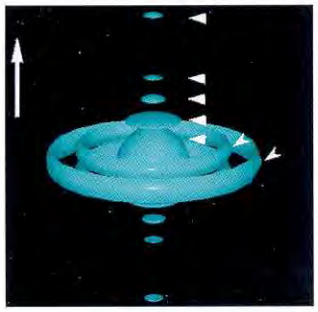

(a)

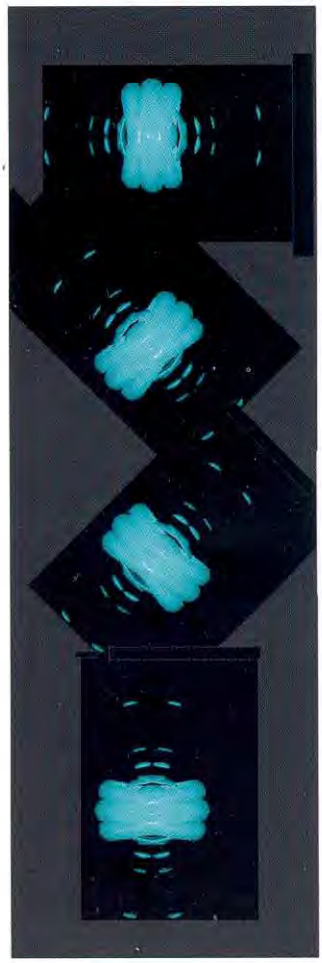

(b)

Figure 7: (a) Model of the Fourier transform associated with the fibres in the egg case laminae. On the fibre axis (directed as the vertical arrow on the top-left side) there are 80 nm repeat reflections, which were inferred from the calculated Fourier transform of the egg-case micrographs. The chevrons indicate rings arising from the meridional and off-meridional reflections, once again inferred from the transforms of the micrographs. These rings are due to random orientation of the fibres around their axes. (b) Models obtained by allowing two main fibril orientations about ± 15° apart along four main directions which are themselves 45° apart. The final Fourier model of the fibrils in the dogfish egg case wall is given by the sum of these models. The meridional rings are omitted for clarity.

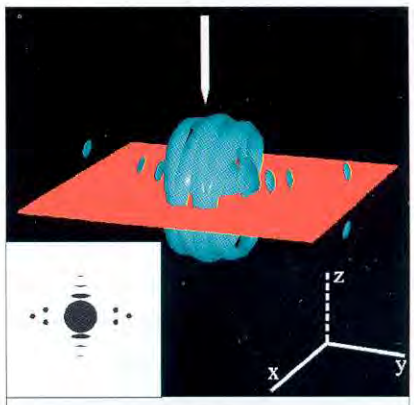

(a)

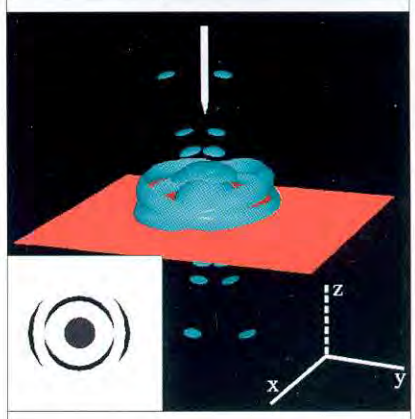

(b)

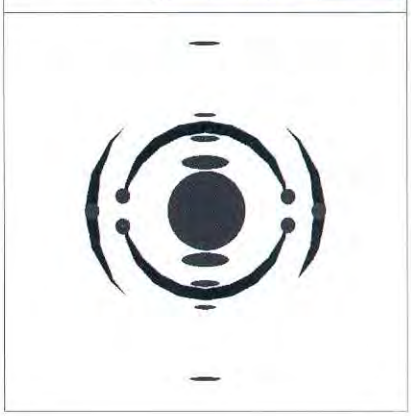

(c)

Figure 8: Origin of the diffraction pattern of Figure 6(b). Fibres which are 15° apart and with horizontal 'average' direction (a) generate the pattern in (b) when they intersect the Ewald sphere (a portion of which is drawn in red in (a)). Fibres oriented vertically (c) give the pattern in (d). If both main fibre directions are present in the specimen, the sum of the two diffraction patterns will be recorded (e). The 10 nm arcs are not prolonged to the equator as they are generated partially by the upper off-meridional reflection ring of the Fourier transform and partially by the lower off-meridional reflection ring (see Figure 7(a)). The gap between the two rings results in the gap between the two 10 nm arcs. Other fibre orientations that lie on the plane generated by the directions of the two fibres previously described are allowed, if the diffraction pattern given by these fibres does not intersect the Ewald sphere except at the 10 nm and 7 nm spot positions.

specimen, the sum of the two diffraction patterns will be recorded (see Figure 8(e)). The 10 nm arcs are not prolonged to the equator as they are generated partially by the upper off-meridional reflection ring of the Fourier transform and partially by the lower off-meridional reflection ring (see Figure 7(a)). The gap between the two rings results in the gap between the two 10 nm arcs. Other fibre orientations that lay on the plane generated by the directions of the two fibres previously described are allowed, if the

diffraction pattern produced by these fibres does not intersect the Ewald sphere except at the 10 nm and 7 nm spot positions.

The other two patterns (Figure 6(a) and (c)) can easily be generated in an analogous way if Fourier space includes the models generated by fibres whose axes lie on planes 45° apart and also have an angular spread around these preferred directions of ±15°. The intersecting Ewald sphere has to be oriented according to the new direction of incidence of the X-rays against the case wall.

Conclusions

The X-ray diffraction patterns can be explained with the hypothesis that the direction of the fibre axes lies in the plane of the laminae and that all the fibres are oriented along a preferred direction within a single lamina. In views down the perpendicular to the laminae, each lamina contains fibrils grouped with a 15° spread of angles around this preferred direction. In views parallel to the laminae, the fibres must be nearly parallel. Successive laminae are arranged with their preferred direction separated by multiples of about 45° (Figure 9). Further, the molecular arrangement seen in the electron microscope is sufficient to explain all of the X-ray diffraction data, suggesting that it is the only one present in any quantity in the egg case wall.

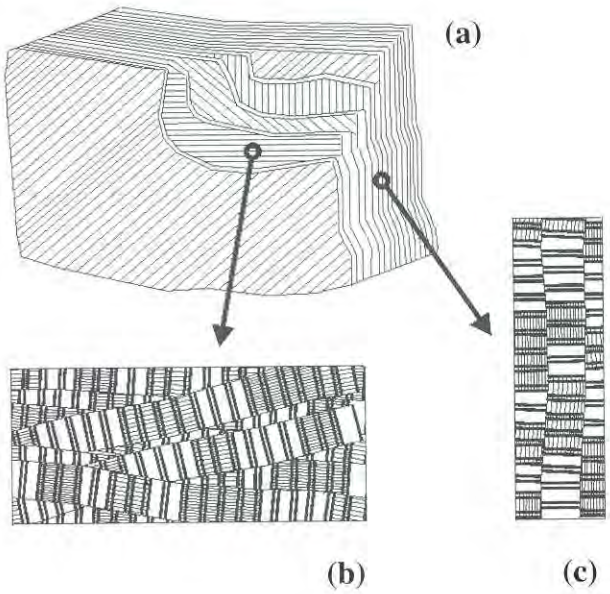

Figure 9: Fibril arrangement in the egg case wall. (a) Portion of the wall showing the changing preferred orientations of the fibrils in successive laminae. Such laminae are about 0.5 μm thick and the orientation change is usually an odd multiple of 45°. (b) Fibril arrangement in a portion of a lamina viewed face-on. The fibrils are about 100 nm in diameter and show preferred orientation with a large spread around this preferred direction of up to ± 15°. Along each fibril, there is only short range order and fibrils show a variable amount of local twisting. Successive pairs of stripes are 40 nm apart. (c) Side view of the arrangement in (b), in which the fibril orientation is almost parallel to the plane of the laminae with only a small degree of orientation.

The egg case wall presumably has many properties in common with the basal lamina in that it has both structural and filtering properties. It may be that the molecular arrangement in the egg case wall will provide insights into the nature of other open network collagens such as type IV, type VI and VIII collagens. It might help to show how type IV collagen influences vital physiological processes such as ultrafiltration in the basal membranes in the kidneys or how the abnormal molecular arrangements in the eyes come to existence.

References

[1] Farquhar, M.G., in *Cell Biology of Extracellular Matrix* (Plenum Press, New York, 1981).

[2] Garner, A., Sarks, S. and Sarks, JP., in *Pathobiology of Ocular Disease* (Marcel Dekker Inc., New York, Basel, Hong Kong, 1994).

[3] Hosney, D., *Experientia* (1978) **34**, 231-40.

[4] Knight, D.P. and Hunt, S., *Nature* (1974) **249**, 379-380.

[5] Rusaouen, M., Pujol, JP., Bocquet, J., Veillard, A. and Borel, JP., *Comp. Biochem. Physiol. B* (1976) **53**, 239-243.

[6] Luong, T.T., Boutillon, M.M., Garrone, R. and Knight, D.P., *Biochemical and Biophysical Research Communication* (1998) **250(3)**, 657-663.

[7] Knight, D.P., Feng, D. and Stewart, M., *Biological review of the Cambridge Philosophical society* (1996) **71(1)**, 81-111.

[8] Feng, D. and Knight, D.P., *Tissue and Cell* (1994) **26**, 155-167.

[9] Feng, D. and Knight, D.P., *Tissue and Cell* (1994) **26**, 385-401.

[10] Knupp, C., Chew, M.W.K., Morris, E.P. and Squire, J.M., *Journal of Structural Biology* (1996) **117**, 209-221.

[11]Knupp, C., Chew, M.W.K. and Squire, J.M., Journal of Structural Biology (1998) **122**, 101-110.

[12] Knupp, C. and Squire, J.M., *Proc. R. Soc. Lond. B.* (1998) **265**, 2177-86.

Fibre Diffraction Experiments with Micron-Sized Beams

M. Burghammer

European Synchrotron Radiation Facility B.P. 220, F-38043 Grenoble Cedex, France.

Scanning diffractometry with beam sizes down to about 2 microns can be used to map hierarchical structures such as polymer fibres or biopolymers. Instrumentation developed at the ESRF microfocus beamline is based on an undulator source, a double focusing mirror and post collimation by collimators or glass capillaries. The method has been applied to a range of topics from spherulitic structures to human hair. Recent instrumental developments suggest that SAXS and WAXS experiments can be performed using a very simple single detector setup. Due to the focusing of the beam, the SAXS resolution is, however, limited to about fifty nanometers. In principle the high flux density allows the investigation of single crystals or very highly textured samples which were accessible until now only to fibre diffraction. Typical cases are chitin and amylose. Techniques developed to study such samples will be discussed.

Tobacco Mosaic Virus as a Model for Phasing and Refinement in Fibre Diffraction

G. Stubbs

Vanderbilt University.

Tobacco mosaic virus (TMV) has the largest asymmetric unit of all structures solved so far by fibre diffraction at atomic resolution. TMV is exceptionally stable, and easily oriented. For these reasons, it has been a model for the development of fibre diffraction methods for more than sixty years. The first diffraction patterns from TMV, and the first recognizably non-crystalline fibre diffraction patterns, were obtained by Bernal and Fankuchen in 1936.

TMV was the first fibre diffraction system in which the isomorphous replacement method was used, only one year after its first use in protein crystallography. Franklin and Caspar independently determined the radial density distribution of the virus; twenty years later we used a multi-dimensional analysis of data from six heavy atom derivatives to solve the cylindrically averaged phase problem.

In the past 15 years, TMV has been a model for the use of macromolecular crystallographic refinement methods in fibre diffraction. Restrained least-squares methods were adapted and used to refine the structure of TMV; molecular dynamics methods were later used to refine several other tobamovirus structures. Current work is focused on developing methods of refining structures against undeconvoluted data, in which the disorientation is too great to allow separation of layer line intensities.

High Resolution Definition of the Axial Molecular Packing of Fibrillar Type I Collagen. A Model Independent Phase Determination

J.P. Orgel, T.J. Wess and A. Miller

DBS University of Stirling. Stirling. FK9 4LA UK.

A high resolution definition of the projected axial structure of collagen presents detailed information about the conformation of the non-helical telopeptides, the relative ratio of the gap/overlap period, and the axial alignment of the collagen molecules within the microfibril. The information needed to define such a structure is contained within the meridional Bragg reflections. However, the majority of previous studies of collagen structure, whether utilising this information or not, have been negatively biased by their model dependent nature. It has been demonstrated in this study, that it is possible to phase the meridional diffraction pattern of type I collagen in an unambiguous way through isomorphous addition. Diffraction data have been recorded using synchrotron radiation sources, and isomorphous derivative proteins have been made

with the minimum of labelling sites. Over 100 meridional intensities have been used to produce a one dimensional electron density map of a single D-repeat of the collagen fibril. From this, the conformation of the N and C telopeptides have been determined within the tight constraints allowed by the derivative labelling shown through difference Fouriers and the 1-D real space model of the native protein. It has been shown that the five collagen chains are equally aligned each containing 234.2 amino acids within the axial unit cell, and that the C-terminal telopeptide is in a folded conformation whilst the N-terminal telopeptide is contracted.

[1] Wess, T.J., Hammersley, A.P., Wess, L. and Miller, A., *J. Mol. Biol.* (1998) **275**, 255-267.

[2] Bradshaw, J.P., Miller, A. and Wess, T.J., *J. Mol. Biol.* (1989) **205**, 685-694.

[3] Hulmes, D.J.S., Miller, A., White, S.W. and Brodsky Doyle, B., *J. Mol. Biol.* (1977) **110**, 643-666.

Fibrillin: A Basis for Tissue Elasticity and Recoil

T.J. Wess, P.P. Purslow and C.M. Kielty

University of Stirling.

Fibrillin is an extracellular protein found to be present in many locations where elasticity is required. It is found in almost pure form in the zonular filaments of the mammalian eye. Molecular assemblies of fibrillin molecules form beaded structures that exhibit apparent variability which may be responsible for the elastic response. This was tested by X-ray diffraction since the changes in the fundamental periodicity of the fibrillin microfibrils would be shown by changes in the meridional diffraction pattern. X-ray diffraction revealed a low angle pattern consisting of eight low angle meridional reflections. The intensity distribution was found to change with the removal of calcium by chelation. The changes in the fundamental period were also not straightfoward. Tissues such as zonular filaments appear to contain two types of fibrillin microfibril packing. Firstly, there are regions of well defined molecular stagger that act as molecular junctions maintaining the tissue integrity, with secondly regions of variable bead length that only make a contribution to diffraction when calcium is removed.

Squeezing Information From Non-Crystalline Diffraction

W. Fuller[1], A. Mahendrasingam[1], C. Martin[1], D.J. Blundell[2], G. Eeckhaut[2], R.J. Oldman[2], D.H. MacKerron[3] and J.L. Harvey[3]

1 Department of Physics, Keele University, Keele, Staffs ST5 5BG.
2 ICI
3 DuPont

The advent of X-ray synchrotron radiation sources has dramatically increased the range and detail which can be obtained in X-ray scattering studies of partially ordered materials. This presentation will illustrate these development with examples from following areas:

(i) characterisation of pathways in strain-induced crystallisation of polymer materials;

(ii) structural variation in polymer materials at high spatial resolution;

(iii) correlation of stress-strain data with small angle scattering in micro-deformation of polymer materials;

(iv) effect of various protocols for biaxial drawing of polymer materials on molecular organisation.

Hard X-Ray Microscopy: Micro-Diffraction, Imaging and Spectroscopy with Coherent Synchrotron Radiation

A. Snigirev

ESRF, B.P. 220, 38043 Grenoble Cedex, France.

The last several years have seen a tremendous breakthrough in the development of microoptics for high energy X-rays. The very low divergence and source sizes of the ESRF beams allow efficient focusing down to a submicron spot sizes using Bragg-Fresnel Optics, Fresnel Zone Plates and Compound Refractive Lenses. Recently

commissioned at the ESRF on ID 22, the Micro-fluorescence, imaging and diffraction (μ-FID) beamline is devoted to the study of samples at the micron and submicron scale in the energy range from 5 to 60 keV. A new flexible setup has been designed to allow the use of the beam after a system of flat mirror and fixed-exit vertically deflecting double-crystal monochromator. Optical components were carefully optimized to conserve the coherence properties of the beam, allowing the observation of holographic patterns of low-density materials. All probes can be used either in the single spot or mapping mode with a sub-μm scanning precision. The methods of investigation comprise microdiffraction (SAXS, WAXS), spectroscopy (XRF, XAS, fluorescence tomography) and imaging (phase contrast imaging/tomography, holography, topography, interferometry). The availability of the hard X-ray microscopy techniques is opening up research opportunities for a broad range of disciplines from semiconductor device engineering to biomedical applications. Results from enviromental, medical and biological sciences will be presented.

Analysis of Time-Sequence Data with FIT2D

A.P. Hammersley

ESRF, B.P. 220, 38043 Grenoble Cedex, France.

High brilliance 3rd generation synchrotron radiation sources combined with the collection efficiency of on-line area detectors mean that time-resolved scattering and diffraction experiments generate large quantities of data. Automated analysis of these data is highly desirable. User interaction, however, remains important to allow versatile masking of contaminating features, etc.

In FIT2D the "FILES SERIES" option "INTEGRATE" has been developed to allow the combination of interactive data analysis and subsequent automated analysis. Raw data may optionally be corrected for detector distortions, and integrated to 1-D 2-theta scans with user defined masking. After successful integration of the first image the integration is repeated automatically for subsequent images.

Small-Angle Diffraction from Mesophases in Colloidal Dispersions of Plates

A.R. Rennie, A.B.D. Brown, C. Ferrero and T. Narayan

Chemistry, King's College London, U.K.
Dept. Phyics, Cambridge, U.K.
ESRF, Grenoble, France.

Small-angle scattering of X-rays and neutrons has been used to investigate the structure in dispersions of plate-like colloidal particles. A model system of monodisperse hexagonal plates of $Ni(OH)_2$ has been prepared. It can be stabilised with polyacrylate to provide almost hard particle interactions. The diffraction pattern has allowed us to show that at high concentrations there is a columnar phase and, at lower concentrations, there is a region of coexistence with a less ordered phase. The possibility of a cubic phase as an intermediate state before an isotropic liquid phase is found at the lowest concentrations is being investigated. The benefits of SAXS and SANS for different aspects of the study will be mentioned. Work on shear alignment of the structures has led to an observation of a phase change to a layer structure.

Transient Liquid Crystallinity in the Drawing of Polyesters

G. Welsh[1], D. Blundell[2] and A. Windle[1]

1 Department of Materials Science and Metallurgy, Cambridge University.
2 Materials Research Centre, ICI, Wilton.

The discovery of a transient smectic phase in random co-polymers of PET and PEN in samples quenched while they were being drawn opened up new levels of understanding and new lines of enquiry:

(a) The slower crystallisation of the random copolymers made the experiment more easy than with the parent homopolymers.

(b) The same effect was observed in the parent homopolymers, although the temperature window from which the quench had to be

performed became more critical. It provided compelling confirmation of previous, somewhat scattered, reports.

(c) Collaboration with Watson Fuller and his group enabled on line confirmation of the appearance of the phase.

(d) The conversion of the smectic phase to the crystalline phase in PET rich members of the series, provides an explanation of the cause of the so-called c-tilt effect well known in PET.

(e) The different response of PEN rich samples to the smectic/crystal transition, provides an explanation of the continuous layer line background, well recognised as a characteristic of the crystalline pattern, while at the same time accounting for the absence of c-shear in this class of sample.

The paper will discuss the findings in the context of on going work.

Reaction Induced Phase Separation: Smart Polymer Processing

Y. Ishii and A.J. Ryan

Department of Chemistry, University of Sheffield, Sheffield, S3 7HF.

Poly(2,6-dimethyl-1,4-phenylene ether) (PPE) is difficult to process without the use of solvents. PPE was dissolved in epoxy resin and reaction induced phase separation in the blend was studied using a time-resolved, small-angle light-scattering camera equipped with an optical DSC. Laser light scattering measurements characterize the subsequent spinodal decomposition process. A four-stage model is discussed: (a) onset of phase separation, (b) early stage of spinodal decomposition, (c) late stage of spinodal decomposition, and (d) apparent phase dissolution. Cahn-Hilliard linear theory, yielding initial correlation lengths and effective interdiffusion coefficients, accounts for the early stage of the spinodal decomposition. In the late stage, the scattering peak maximum, q_m, starts to decrease with time according to a power-law. However, the maximum in the scattered intensity, I_m, does not satisfy a power-law due to the large change in the epoxy refractive index during crosslinking. The phase-inverted morphology and mechanical properties of the cured blend are investigated by SEM, TEM and DMTA.

Neutron Scattering Studies of the Effect of Ca^{2+} on the *In Situ* Structures of Troponin I and Troponin C

P.A. Timmins[1], D. B. Stone[2], D.K. Schneider[3], I. Krylova[2] and R.A. Mendelson[2]

1 Institut Laue-Langevin, BP156, 38042 Grenoble Cedex 9, France.
2 Cardiovascular Research Institute and Dept. of Biochemistry and Biophysics, University of California, San Francisco, CA 94143-0130, USA.
3 Biology Dept., Brookhaven National Laboratory, Upton, NY 11973, USA.

Neutron small-angle scattering using contrast variation is a powerful method to determine the quaternary structure of biological macromolecular complexes. If the complexes have natural internal contrast due to having components of different chemical composition (*e.g.* proteins and nucleic acids) then contrast matching can be attained through the use of appropriate H_2O/D_2O mixtures. In cases where this is not so then deuteration of parts of the complex by disassembly and reassembly of specifically *in vivo* deuterated components can be used. We have used this latter technique to investigate the *in situ* structures of troponin C (TnC) and troponin I (TnI) in whole troponin and the influence of regulatory amounts of Ca^{2+} on these structures. In separate difference experiments, 97% deuterated TnC and TnI within whole troponin were studied with and without Ca^{2+} in 41.6 mole % buffers in which protonated sub-units are invisible. The radius of gyration (R_g) of TnI was found to decrease by ~10% on addition of regulatory calcium indicating a significant compaction of the structure. The cross-sectional radius of gyration (R_c) increased by ~9% under the same conditions. Modelling

studies showed that the high-Q scattering could be fit by a TnI molecule consisting of two domains; one a highly oblate ellipsoid of revolution containing about 65% of the mass, the other a highly prolate ellipsoid. Similar experiments with deuterated TnC demonstrated that it was elongated *in situ* and that its radius of gyration was not sensitive to the Ca^{2+} occupancy of its regulatory sites. The cross-sectional radius of gyration did increase with Ca^{2+} addition in a manner expected from crystallographic and NMR studies of the isolated TnC.

X-Ray Diffraction Probing of Molecular Events During Muscle Contraction

J.J. Harford*, C. Knupp and J.M. Squire

Biological Structure and Function Section, Biomedical Sciences Division, Imperial College School of Medicine, London SW7 2AZ.
*Present address: SPring8, JASRI, 323-3 Mihara, Mikazuki-cho, Sayo-gun, Hyogo 679-5198, Japan.

Although there are several distinct biological molecular motors, striated muscle has great advantages in structural studies since the highly oriented, force-producing filaments actin and myosin are distributed regularly and at high concentration through macroscopic volumes of tissue [1]. It is therefore possible with muscle, as with no other molecular motor, to study the structural behaviour of the interacting molecules in a fast, time-resolved mode, using synchrotron radiation, optimised low-angle beam-lines and state of the art X-ray detectors [2]. Currently, the Daresbury SRS, low-angle beam-line 16.1, and the RAPID multiwire area detector together provide a world-beating combination. Although the SRS is no longer a state of the art source, no third generation synchrotrons, such as ESRF, SPring8 or APS, have detectors that are close in their count-rate capabilities to RAPID. When the UK's new DIAMOND synchrotron is a reality, beamlines equivalent to 16.1 together with RAPID detectors will permit time-resolved X-ray diffraction studies of dynamic biological (and other) systems to be carried out with unprecented accuracy and reliability. In the present study we have been attempting to monitor the sequence of events involved in muscle activation and regulation [2,3,4]. In a typical experiment a highly ordered 'fin' muscle from plaice is electrically stimulated at time zero with a 50 Hz AC field to give a sustained tetanic contraction. During the roughly 150 to 200 ms tension rise time the muscle's low-angle diffraction pattern is monitored in 1 ms time bins. This is compared with longer exposures both before activation and at the tension plateau of the tetanus. Tension relaxation following cessation of the stimulus field was monitored in 2 ms time bins. The general structure of this muscle [1,3] and the molecular changes involved in the control and production of force in the plaice contractile cycle will be described [2,4]. In particular the change of the equatorial (1,1) reflection is rather fast, compared with the changes of the equatorial (1,0) reflection and tension, which have about the same time-courses. The meridional 14.3 nm reflection changes at an intermediate rate. The relative speed of the change of the actin second layer-line, indicative of activation events, is being determined and will be described.

[1] Squire, J.M., *Curr. Opinion Struct. Biol.* (1997) **7**, 247-257.
[2] Harford, J.J. and Squire, J.M., *Rep. Prog. Phys.* (1997) **60**, 1723-1787.
[3] Hudson, L., Harford, J.J., Denny, R.C. and Squire, J.M., *J. Mol. Biol.* (1997) **273**, 440-455.
[4] Squire, J.M. and Morris, E.P., *FASEB J.* (1998) **12**, 761-771.

Unit Cell Structure and Intermolecular Interactions in *Lethocerus* Fibrillar Insect Flight Muscle in Defined States

H.A. AL-Khayat[1], J.J. Harford[1,2], M.K. Reedy[3], T.C. Irving[4] and J.M. Squire[1]

1 Biological Structure and Function Section, Biomedical Sciences Division, Imperial College School of Medicine, London SW7 2AZ.
2 Experimental Research Division, SPring-8, 323-3 Mihara, Mikazuki-cho, Sayo-gun, Hyogo 679-5198, Japan.
3 Department of Cell Biology, Duke University, Durham, NC 27710, USA.
4 Department Biological, Chemical and Physical Sciences, Illinois Institute of Technology, Chicago IL, 60616.

In the interest of studying the molecular structure and function of muscle, we are trying to determine the

3D structure of actin and myosin filaments and the structural changes underlying contraction and its regulation. Our main approach involves using methods developed in a BBSRC-funded study of fish muscle (Hudson *et al.*, 1997). Here these methods are being used to solve the full unit cell structure in relaxed insect flight muscle and also rigor insect muscle. Actin molecules and myosin heads are particularly well organized in insect flight muscles and give rise to semi-crystalline low-angle X-ray diffraction patterns.

Our group at Imperial College have already analysed and solved the structure of myosin filament in relaxed insect flight muscle (Hudson *et al.*, in preparation). We are now refining this structure and propose to apply these methods to solve the full unit cell, including the actin filaments with troponin and tropomyosin, in both relaxed and rigor insect flight muscle using new X-ray diffraction data. This will provide direct information on the actin-myosin interface and also on the conformation and the flexibility of the muscle heads in different defined sates.

Initial studies (Hudson *et al.*, in preparation) on modelling the structure of the myosin filament in relaxed insect flight muscle to 7.0 nm resolution using the myosin head shape of Rayment *et al.* (1993) and the simulated annealing procedure of Hudson *et al.* (1997), gave a crystallographic R-factor of 5.97 % against 65 reflections with the resting crossbridges projecting at 90° to the filament long axis as originally reported by Reedy *et al.* (1965).

In this meeting, we will present a poster showing our latest results on this project.

[1] Hudson, L., Harford, J.J., Denny, R.C. and Squire, J.M., *J. Mol. Biol.* (1997) **273**, 440-455.

[2] Hudson, L., Denny, R.C., Harford, J.J., Reedy, M.R., Irving, T.C. and Squire, J.M., in preparation.

[3] Rayment, I., Rypniewski, W.R., Schmidt-Base, K., Smith, R., Tomchick, D.R., Benning, M.M., Winkelmann, D.A., Wesenberg, G. and Holden, H.M., *Science* (1993) **261**, 50-58.

[4] Reedy, M.K, Holmes, K.C. and Tregear, R.T., *Nature* (1965) **207**, 1276-1280.

X-Ray Camera for Wide-Angle X-Ray Diffraction Studies of the Biaxial Deformation of Polymers

S.J.Bingham, A.Mahendrasingam, C.Martin, J.L.Harvie, D.H.MacKerron, W.Fuller and C.Riekel

Department of Physics, Keele University, Staffordshire, ST5 5BG, UK.
DuPont UK Ltd, PO Box 2002, Wilton, Middlesbrough, Cleveland, TS90 8JF, UK.
ESRF, BP 220, F-38043,Grenoble Cedex,France.

An X-ray fibre diffraction camera capable of biaxial deformation of polymer films, has been developed in the Physics Department of Keele University. The camera allows time-resolved X-ray studies of the change in orientation and crystallinity at draw rates of up to $12s^{-1}$ and draw ratios of up to 6:1 to be recorded. The application of the camera in the study of biaxial deformation of poly(ethylene terephthalate) (PET) during experiments on synchrotron and laboratory sources is described.

An Age-Dependent Study on the Effects of Photorefractive Keratectomy on Rabbit Cornea, using Transmission Electron Microscopy and X-Ray Diffraction Techniques

C.J. Connon[2], K.M. Meek[1], A.L. Patmore[3], J. Marshall[3] and R.H. Newton[1]

1 Cardiff University, Cardiff, UK.
2 The Open University, Oxford Research Unit, Oxford, UK.
3 St Thomas' Hospital, London, UK.

Corneal transparency is due to the uniformly small diameter collagen fibrils and to the high degree of ordering in their lateral arrangement. Photorefractive keratectomy (PRK) is a surgical technique in which a laser is used to re-shape the front surface of the cornea and thus produce a refractive change to compensate for the effects of (usually) myopia. Previously, corneal haze following PRK has been studied using young rabbits. To look for an age-

related response, we have measured haze in young (2.5kg) and old (5kg) rabbits. The right eyes of 8 rabbits were subjected to PRK using an argon-fluoride excimer laser (193nm). Objective measurements of haze were made at various time intervals during wound healing. The anterior stroma (0-2μm below the epithelium) was studied to predict the transmission of visible light through the wounded corneas. The haze measurements showed that old rabbits had an increased response that peaked at 23 days post-surgery, but over the longer term (12 months) the haze levels were similar. Electron microscopy revealed that, 8 months after surgery, there was a large zone, up to 2μm thick, of irregularly spaced and poorly oriented collagen fibrils directly below the epithelium. X-ray diffraction measurements were used to determine the fibril refractive index and to scale up electron micrographs to account for shrinkage during preparation for microscopy. The relative positions and diameters of the individual fibrils were obtained from the scaled micrographs and the Direct Summation of Scattered Fields model (Freund, D.E. *et al., Appl. Optics* (1986) **25**, 2739-2746) was used to predict the transmission of visible light through the anterior of the cornea. There was no significant predicted increase in light scattering in either young or old rabbits following PRK. Disorder in the newly deposited collagen does not, therefore, explain the observed post-operative haze.

The Micro-SAXS Facility at the ESRF-Beamline ID22

M. Drakopoulos, A. Snigirev, I. Snigireva

ESRF, BP 220, F-38043,Grenoble Cedex, France.

ESRF beamline ID22 is designed for microscopic studies of material's properties with hard X-rays. Basic elements are focusing and imaging optics through which sub-micrometer resolution is obtained. Besides direct imaging and various micro-spectroscopic methods, micro-diffraction fits into the beamline activities. In this context a micro-SAXS camera has been set up recently and has been tested in a series of experiments.

The micro-SAXS camera consists of a Fresnel Zone plate, a collimating system and CCD-based area detectors. X-rays of energy around 10 keV are focused to 2 μm (vertical) by 10 μm (horizontal) at the sample position with a flux of 5×10^{10} ph/s. The lens-sample distance is 1300 mm. The divergence after the lens is 5×10^{-4} yielding a resolution in momentum transfer of 0.01 nm^{-1}. Currently the collimator limits the minimum momentum transfer to 0.05 nm^{-1}. Two 2D detectors are available with a DQE of 0.5 (0.7) and an active area of 35 mm (100 mm) diagonal. The pixel size is 23 μm (58 μm), the dynamic range is 16 bit. The detectors have a dark-noise of 100 counts/pixel. The radiation background is in the range of the detector's noise. The sample-detector distance can be varied between 30 mm and 2m. Sample alignment can be accomplished with an optical microscope online. Because of suitable lens-sample distances, samples can easily be changed and handled.

With this micro-SAXS camera, local diffraction patterns of collagen fibres (rat-tail tendon) have been collected. Significant intensity of 1st to 20th diffraction orders was collected in a 30 seconds exposure. Scattering from diluted calcification volumes along the mineralisation direction of growing bone was recorded with micrometer spatial resolution.

In future the detectable minimum momentum transfer will be improved.

Templated Crystallisation: Soft Phases Controlling Hard Materials

J.P.A. Fairclough[1], A.J. Ryan[1], N.J. Terrill[1], L. Messe[1], S. Turner[1], S-M. Mai[2], C. Booth[2] and W. Bras[3]

1 Department of Chemistry, University of Sheffield, Sheffield, S3 7HF.
2 Department of Chemistry, University of Manchester, Manchester, M13 9PL.
3 DUBBLE, ESRF, Grenoble.

Throughout nature, the structure of hard materials *e.g.* coral, is controlled by a soft template. We have examined crystallisation in shear oriented block

copolymers, where a soft phase of microphase separated melt controls the preferred direction of crystallisation. In lamella phases, the comparison is simple and direct over a range of molecular weight and domain sizes. For hexagonally arranged cylindrical systems and for cubic gyroid structures, the choice of preferred directions is limited. We have used real time SAXS to monitor the structure formation upon crystallisation. Results will be presented for recent measurements on stations 16.1 and 2.1 and at DUBBLE at the ESRF.

Crystallization and Morphology Development in Oriented Poly(Ethylene Terephthalate) and Related Copolymer Films

E.L. Heeley[1], D.J. Hughes[2], A. Mahendrasingam[3], W. Fuller[3], D.H. MacKerron[4], R. Pendlbury[5] and A.J. Ryan[1]

1 Department of Chemistry, University of Sheffield, Sheffield, S3 7HF.
2 Department of Civil and Environmental Engineering, University of Salford, Salford, M5 4WT.
3 Department of Physics, Keele University, Keele, Staffordshire, ST5 5BG.
4 Dupont (UK) Ltd, PO Box 2002, Wilton Centre, Wilton, Middlesbrough, Cleveland TS9 8JE.
5 ICI Wilton Research Support Group, PO Box 90, Wilton, Middlesbrough, Cleveland TS90 8JE.

The molecular morphology of several oriented poly(ethylene terephthalate) (PET) and copolymer films have been investigated using Small- and Wide-angle X-ray Scattering (SAXS/WAXS) techniques at the Daresbury Synchrotron Radiation Source (SRS). The films were uniaxially deformed in a purpose built instrument to mimic typical industrial processing conditions. During sample deformation, synchronized SAXS/WAXS data were collected using a 2-D gas-filled multiwire area detector and a portable CCD based area detector respectively.

The samples were deformed at a rate of 24000% min^{-1} at 85°C, then step annealed up to a temperature of 220°C. The 2-D X-ray data obtained were used to explore the morphological changes in the samples as annealing progressed. The 2-D SAXS data were used to determine detailed information pertaining to the samples' changing crystallinity and lamellar structure. This information was obtained by using a purpose written 1-D correlation function analysis package known as *corfunc*. The X-ray data were also coupled with physical density measurements of the films to ascertain their crystallinity as a comparative method.

From the X-ray and physical analysis of the PET films deformed under industrial processing conditions, it has been possible to evaluate the changes in crystallinity and lamellar structure during annealing. The results indicate that the homopolymer PET sample displays differences in the development of crystallinity and lamellar structure compared to that of the copolymer samples. Generally, the homopolymer sample has increased crystallinity compared to certain copolymer samples, leading to initial conclusions that the addition of only a small fraction of comonomer has the ability to significantly change the morphology of a PET film during processing.

Effect of pH and Calcium, Phosphate and Phosphopeptide Concentrations on the Size and Substructure of Calcium Phosphate Nanoclusters as Determined by X-Ray and Neutron Scattering and Circular Dichroism Spectroscopy

C. Holt[1], T. Drakenberg[2], N. Errington[3], C.G. de Kruif[4], J. Leaver[1], P.A. Timmins[5], R. Tuinier[4] and N.M. Wahlgren[2]

1 Hannah Research Institute, Ayr, Scotland, KA6 5HL, UK.
2 Physical Chemistry 2, University of Lund, Sweden.
3 National Centre for Macromolecular Hydrodynamics, University of Leicester, UK.
4 NIZO food research, Ede, The Netherlands.
5 Institut Laue-Langevin, Grenoble, France.

The ability of casein in the form of colloidal-sized casein micelles to modulate the phase separation of calcium phosphate during milk secretion was adapted to produce nm-sized particles of calcium phosphate stabilised by a 25 amino acid N-terminal tryptic phosphopeptide of bovine ß-casein (nanoclusters). The nanoclusters were prepared from an undersaturated solution of salts and the peptide by raising the pH homogeneously from about 5.5 to 6.7

with urea plus urease. Chemical analysis, multinuclear nmr and infrared spectroscopy showed that they comprise an amorphous dicalcium phosphate bound to the phosphopeptide.

Calcium phosphate nanoclusters were prepared under standardised conditions using 10 mg ml^{-1} of the phosphopeptide as stabilising agent. The molecular mass determined by sedimentation equilibrium was 197,600±13,700 and the apparent radius of gyration determined by X-ray scattering was 2.80±0.05 nm. A small angle neutron scattering contrast variation study in $1H_2O$-$2H_2O$ mixtures was performed and gave radii of gyration at the calculated match points for the calcium phosphate (88.2% $2H_2O$) and phosphopeptide (41.3% $2H_2O$) of 3.39±0.08 nm and 1.85±0.05 nm respectively. Measurements at larger scattering wave vector showed a subsidiary maximum at about $Q = 1.6\ nm^{-1}$.

The results are consistent with a model of the nanoclusters comprising a spherical core of 355±20 $CaHPO_4.2H_2O$ units, density 2.31 g ml^{-1} and radius 2.30±0.05 nm, surrounded by 49±4 peptide chains with a partial specific volume of 0.7 cm^3g^{-1}, forming a tightly packed shell with an outer radius of 4.04±0.15 nm.

Subsequent contrast variation neutron scattering and X-ray scattering measurements on smaller and larger nanoclusters indicate that the shell has a constant thickness, but the core size can be varied. The shell thickness cannot be varied by addition of up to 8M urea and the conformation of the peptide in the shell and in free solution appears to be mostly non-regular, as measured by far UV CD spectroscopy.

The phosphopeptide is able to arrest the process of growth of the precipitating phase of calcium phosphate at its earliest stages. The ability of casein to form nanoclusters in milk suggests a more general mechanism for avoiding pathological calcification and regulating calcium flow in tissues and biological fluids exposed to or containing high concentrations of calcium.

[1] Holt, C., Wahlgren, N.M. and Drakenberg, T., *Biochemical Journal* (1996) **314**, 1035-1039.
[2] Holt, C., Timmins, P.A., Errington, N. and Leaver, J., *European Journal of Biochemistry* (1998) **252**, 73-78.

A Flexible, Integrated Approach to *In Situ* Resolving X-Ray Diffraction Studies of Polymer Systems

J.J. Holt and G.R. Mitchell

Department of Physics, University of Reading, Whiteknights, Reading RG6 6AF, UK.

DualAXIS is a fully integrated system developed around a CCD-based area detector, which allows control over sample environment, image processing, and data analysis through a dedicated PC interface. It has been specifically designed for time resolving *in situ* SAXS (Small-Angle X-ray Scattering) and WAXS (Wide-Angle X-ray Scattering) experiments. The most common mode of operation involves subjecting polymer systems to controlled shear deformations, which simulate industrial processing conditions. A small volume multipurpose shear cell has been designed as a sample mount to operate in the temperature range 25-250°C with gas cooling at a rate of 50°C/sec. The software is window based and runs in a Windows NT environment. It contains both experimental control and data analysis. All aspects of the sample environment including the shear rate and temperature can be programmed. The system allows data to be accumulated in a variety of ways with subsequent or in-line analysis. Experiments may be written in the form of a text command file to allow sequences to run without user intervention for prolonged periods. A variety of flexible analysis tools are provided to facilitate measurement of quantitative structural parameters, orientation, and crystallisation in a defined and automated manner.

Collagen Fibril Compaction Accompanies the Acquisition of Transparency in Developing Chick Corneas

A.J. Quantock

Cardiff University

To study some ultrastructural aspects of developing chick corneas we performed a synchrotron X-ray

diffraction analysis of 22 specimens obtained daily from developmental day 10 through day 19. Before day 12 of development in chicks we were unable to detect a meridional X-ray diffraction pattern from cornea. Neither were we able to record a first-order equatorial X-ray reflection at this time. Normally, these reflections are present in corneal X-ray patterns, arising from, respectively, the periodic axial electron density of fibrillar collagen and the lattice-like arrangement of the fibrils. By day 12 of development we could detect the third- and fifth-order meridional reflections (indicating increased amounts of collagen) and a first-order equatorial reflection (implying that more collagen was regularly arranged). The third- and fifth-order meridional reflections became more intense as the tissue matured, suggestive of a continued deposition of fibrillar collagen, and the scattering angle of the interfibrillar maximum increased, suggesting that regularly arranged collagen was becoming more closely packed with maturation. In embryonic chick corneas, the establishment of an orderly, fairly compacted matrix of collagen fibrils may be one of the main events underlying the acquisition of corneal transparency.

Micro-SAXS and Stress / Strain Measurements during the Tensile Deformation of Single Struts of an Elastomeric Polyurethane Foam

C. Martin[1], G. Eeckhaut[2], A. Mahendrasingam[1], D.J. Blundell[3], W. Fuller[1], R.J. Oldman[3], S.J. Bingham[1], A. Cunningham[2], T. Dieing[4] and C. Riekel[4]

1 Department of Physics, Keele University, Staffordshire, ST5 5BG, U.K.
2 Polymer Science Group, R & D Department, ICI Polyurethanes, Everslaan 45, B-3078 Kortenberg, Belgium.
3 ICI R & T Centre, P.O. Box 90 Wilton Centre, Middlesbrough, Cleveland, TS90 8JE, U.K.
4 ESRF, BP 220, F-38043 Grenoble Cedex, France.

A micro-deformation stage based on a piezoelectric crystal actuator and capable of measuring the force applied to micron-sized polymeric samples is described. Laboratory stress/strain and stress relaxation measurements on a single strut of an elastomeric polyurethane foam have been conducted for the first time. Using this device, micro small-angle X-ray scattering patterns have been collected on the microfocus beamline at the European Synchrotron Radiation Facility, simultaneously with strain and force measurements, during the time-resolved tensile deformation of a single foam strut.

Structural Changes in Tropomyosin and Troponin during Ca^{2+}-Activation of Actin Filaments in Frog Muscle

N. Shing Mok, H. AL-Khayat and J.M. Squire

Biological Structure and Function Section, Biomedical Sciences Division, Imperial College, London SW7 2AZ.

Muscular activity is generated when nerve action potentials, propagated into the muscle via the T-tubular system, cause the release within the sarcoplasm of Ca^{2+} ions [1]. These ions in turn attach to the troponin-C component of the troponin complex on the thin, actin-containing, muscle filaments. Each troponin complex interacts via a 40 nm long tropomyosin molecule with seven actin monomers along one strand of the long-pitch actin helix. Studies in the early 1970s [2-4] suggested that the structural effect of calcium binding to troponin is to change the position of the tropomyosin strands within the "groove" of the actin filament helix, thus uncovering or altering the site on actin to which myosin heads bind in order to produce force and movement. This way of controlling the actin-myosin interaction was soon christened the "Steric Blocking Model". Since that time the atomic structure of the actin monomer and filament have been described [5], and further insights into the tropomyosin shift have been obtained both by X-ray fibre diffraction [5] and by electron microscopy and 3D reconstruction [6]. Unfortunately all of these approaches ignored the possible structural implications of the troponin complex on X-ray diffraction or EM data [7]. Troponin has an axial repeat along the actin filaments of about 38.5 nm which is different from the helical repeats (2.75 nm axial translation, about 2 x 37 nm pitch) of the actin filament. We have established a diffraction modelling program that properly includes the contribution from the troponin complex. Unfortunately the full atomic structure of

the troponin complex has not yet been determined. It is possible that this complex may radically change its conformation when Ca^{2+} ions are bound. New results will be presented using a plausible troponin shape, but to date the implication is that even with the troponin taken into account, an azimuthal shift of tropomyosin as in the original "Steric Blocking Model" may be necessary.

[1] Ebashi, S. and Endo, M., *Biophy. Mol. Biol.* (1968) **18**, 123-183.
[2] Huxley, H.E., *Cold Spring Harbor Symp. Quant. Biol.* (1972) **37**, 361-376.
[3] Haselgrove, J.C., *Cold Spring Harbor Symp. Quant. Biol.* (1973) **37**, 341-352.
[4] Parry, D.A.D. and Squire, J.M., *J. Mol. Biol.* (1973) **75**, 33-55.
[5] AL-Khayat, H.A., Yagi, N. and Squire, J.M., *J. Mol. Biol.* (1995) **252**, 611-632.
[6] Vibert, P.J., Craig, R. and Lehman, W., *J. Mol. Biol.* (1997) **266**, 8-14.
[7] Squire, J.M. and Morris, E.P., *FASEB J.* (1998) **12**, 761-771.

Materials for the Millennium: How Synchrotron Radiation is being used to Research Polymers for the 21st Century

N.J. Terrill, G.P. Diakun and A.J. Gleeson

Daresbury Laboratory, Daresbury, Warrington, Cheshire, WA4 4AD.

Polymers have become an essential part of modern-day life. They have found application in a wide range of areas; including packaging materials such as carrier bags, through to more esoteric uses such as artificial heart valves. At Daresbury, the Non Crystalline Diffraction (NCD) facility has been used to examine many aspects of polymer science. Physical measurements have previously been performed in isolation on polymers to try to understand their properties. With the advent of simultaneous multiple techniques developed at Daresbury, it is now possible to combine these physical measurements with data from both Small- and Wide-Angle X-Ray Scattering (SAXS and WAXS) to better understand the physical processes taking place. For example, the rheological behaviour of polymers is better understood when the structural information is clear. This is also true for processing. Study has included *in situ* experiments examining real industrial processes such as extrusion, by which many plastic products are manufactured. The work carried out at Daresbury has led to a better understanding of polymer crystallisation on the academic level and better polymer products on the commercial level.

X-ray and Neutron Reflectivity of Thin Block Copolymer Films

C. Salou, A.J. Ryan and J.P.A. Fairclough

Department of Chemistry, University of Sheffield, Dainton Building, Sheffield S3 4HF.

Diblock copolymers exhibit different microphase-separated morphologies including spheres, hexagonally packed cylinders and lamellar structures. The relative volume fraction of each block along with the Flory-Huggins interaction parameter (χ) and the degree of polymerisation dictates the phase separation and, thus, the lamellar spacing (d-spacing) in the copolymers. Blends of diblock copolymers with homopolymers have been the subject of many studies. Here our study is based upon the work by Winey and co-workers. They investigated the variation of the block copolymer A-B (in the bulk) morphologies upon addition of homopolymer A or B as a blend. In these blends, the free energy is reduced when the homopolymers segregate to the appropriate domains of the ordered structure reducing the number of unfavourable segmental A/B contacts. The microdomains swell in order to accommodate the homopolymers resulting in transitions from one type of microstructure to another in the process. In this study blends of commercially available asymmetric diblock polystyrene-polybutadiene (PS-b-PB) copolymer (MW=83,500 $gmol^{-1}$) with homopolymer (deuterated and hydrogenated PS) and a symmetric diblock polystyrene-poly(dimethylsiloxane) (PS-b-PDMS) (MW=1,000,000 $gmol^{-1}$) have been investigated. Solutions of PS-b-PB blended with 20wt% PS (h-PS or d-PS) and PS-b-PDMS were

prepared in toluene and used to spin-cast thin films at two different spin-speeds (1500, 3000rpm), onto polished silicon wafers, covered with a native oxide layer. Other samples were produced by simply casting the blends into a mould. The morphology of the thin films was studied using X-ray and neutron scattering techniques. Small-Angle X-ray Scattering (SAXS) was used to investigate the morphology of the cast samples and was conducted on station 2.1 of the Daresbury SRS. The deuterated thin films prepared from the blends were examined using the reflectometer CRISP at ISIS, Rutherford and the reflectometer on station 16.2 at Daresbury SRS. From the SAXS studies, a lamellar morphology is detected in the blends of PS-b-PB with h-PS, as does the bulk sample. The intensity of the scattering increases for the blends due to the addition of the homopolymer and therefore the change of the polystyrene volume fraction in the diblock (*i.e.* volume fraction ratio tends to 50/50). The results from neutron and X-ray reflectivity experiments, were combined to determine the number of layers in the film and the effect of the processing techniques on these layers. Unfortunately for the PS-b-PDMS system, the same investigations were made, but due to the high MW and high d-spacing, the instruments did not have the resolution to produce valuable data at the time. However, further investigations will be conducted on the same polymer system having a lower molecular weight.

Phase Separation Behavior in Commercial Al-Li Alloys. A RT-SAXS Characterization

A. Triolo[1], V. Arrighi[1], F. Lo Celso[2] and R. Triolo[2]

1 Dept. of Chemistry, Heriot Watt University, UK.
2 Dept. of Physical Chemistry, University of Palermo, Italy.

We present novel results on the phase separation occurring in commercial aluminum-lithium alloys. Quenching the samples from a high temperature state down to a low temperature one, phase separation occurs, leading to the formation of a minority phase, which is finely dispersed in the matrix. The kinetics of the growing of the segregated clusters is followed by means of the real time SAXS technique. Results obtained up to now indicate the occurrence of a bimodal growth behavior in the low temperature regime, while SR-SAXS measurements seem to indicate that in the high temperature regime only a single growth mechanism determines the overall development of morphology. Various analysis approaches are presented in order to extract as much information as possible from experimental results. Simple invariant analysis leads to Avrami plots, which show the above-mentioned behaviour. Moreover, data have also been analyzed by fitting the whole scattering curve by means of a structural model.

α-Tocopherol Induces Two Crystal Phases and One Inverted Hexagonal Phase in Aqueous Dispersions of Dipalmitoylphosphatidylethanolamine

X. Wang and P.J. Quinn

Division of Life Sciences, King's College London, Campden Hill, London W8 7AH.

The effect of α-tocopherol on the structure and thermotropic phase behaviour of aqueous dispersions of dipalmitoylphosphatidylethanolamine in mixtures containing 0, 2.5, 5, 10 and 20mol% α-tocopherol was examined using synchrotron X-ray diffraction methods. Dispersions were equilibrated for 24 hours at a temperature below 30°C before measurement. Pure phospholipids only underwent gel to liquid-crystalline phase transition in the initial heating scan. α-Tocopherol-rich domains, however, were observed in all codispersions of phospholipids with α-tocopherol examined and were assigned on the basis of an increase in scattering intensity of the phase in proportion with the concentration of α-tocopherol in the mixture. In the initial heating scan, α-tocopherol-rich domains, characterised by broad lamellar repeat spacings (5.0 nm at 55°C) in the small-angle region, appear at about 40°C and increase in scattering intensity with increasing temperature. The broad lamellar repeat spacings from the α-tocopherol-rich domains were replaced by an inverted hexagonal structure a few degrees below the gel to liquid-crystalline phase transition temperature of the pure phospholipid at 66°C. The intensity and repeat spacing of the inverted hexagonal phase increased with increasing temperature up to the appearance of

the liquid-crystalline phase. Then the intensity of the inverted hexagonal phase began to decrease with increasing temperature up to the disappearance of the gel phase. The repeat spacing of the inverted hexagonal phase remained relatively constant when coexisting with the liquid-crystalline phase, but, with increasing temperature, the scattering intensity increased at the expense of the lamellar liquid-crystalline phase. Two types of crystal phases Lc1 and Lc2 were observed in all codispersions containing α-tocopherol. The Lc1 is characterised by the first four orders of the sharp diffraction indexing a d-spacing ratio 1:1/2:1/3:1/4 in small-angle region with multiple diffractions in the wide-angle region, and Lc2 is characterised by the broad lamellar diffraction in the small-angle region with multiple diffractions in wide-angle region. Static X-ray diffraction indicates that the stoichiometry of phospholipid:α-tocopherol in Lc1 and Lc2 is about 4:1. In cooling scans performed immediately after heating scans, no crystal phases were observed in all codispersions. The results indicate that during the incubation, α-tocopherol molecules in the gel phase concentrate and form the crystal phase domain Lc1 which has a stoichiometry of 4:1 for phospholipid: α-tocopherol. With increasing temperature the hydrocarbon chains of the domain are tilted at more than 35° to the bilayer normal and transform into the Lc2 domains which transform into the inverted hexagonal phase at higher temperature. When cooling down the inverted hexagonal phase directly transforms into gel phase.

Forthcoming Meetings

9th Annual Fibre Diffraction and Non-Crystalline Diffraction Workshop

June 26-28, 2000, University of Sheffield

(Organised by Mark Shotton, Richard Denny and Trevor Forsyth)

[For further information and registration, see the web pages at http://www.dl.ac.uk/SRS/CCP13 or contact m.shotton@dl.ac.uk]

10th London Muscle Conference

September 15, 2000, Imperial College, London

(Organised by John Squire, Nancy Curtin and Pradeep Luther)

[Details from Prof. John Squire j.squire@ic.ac.uk, 0207 594 3185]

3rd Alpbach Workshop on Fibrous Proteins: "Coiled-Coils, Collagen and Co-Proteins"

September 16-21, 2001, Boglerhof Hotel, Alpbach, Austria

(Organised by David Parry, John Squire and Bob Goldman)

[Details from Prof. John Squire j.squire@ic.ac.uk, 0207 594 3185]

DARTS Bursaries

DARTS at Daresbury Laboratory has funded several bursaries for PhD students to attend the 9th Annual Fibre Diffraction and Non-Crystalline Diffraction Workshop at the University of Sheffield (see above and inside back cover). These bursaries will cover the cost of accommodation and registration and may include a contribution to travelling expenses. An application for a bursary can be made through the web pages at http://www.dl.ac.uk/SRS/CCP13

All bursary applications must be accompanied by the submission of a poster abstract to the Workshop.

Fibre Diffraction Review: Instructions to Authors

Submitted original papers, comments/letters or meeting reports for inclusion in *Fibre Diffraction Review* are welcome.

Original Papers:

Suitable topics include technical developments (software or hardware) and new results from fibre diffraction or small-angle scattering experiments (using either X-rays or neutrons).

All papers will be refereed by at least two people (from the CCP13 Committee or their nominated referees) and may be either (a) accepted as they stand, (b) returned for rapid revision, or (c) rejected.

Meeting Reports:

Fibre Diffraction Review includes reports on relevant meetings and conferences which include an element of fibre diffraction or small-angle scattering and which will be of general interest to our readers. Such reports will often be solicited by the Editor from known meeting participants. Other potential contributors to this part of the journal should contact the Editor prior to writing their report.

Comments/Letters:

Feedback from readers about CCP13, the NCD community and about the journal itself are welcome. These could be in the form of comments or letters to the Editor. Suitable contributions will be published in the Journal.

Advertisements:

Industrial/commercial adverts of interest to our readers are welcome. Potential advertisers should contact the Editor for details of current rates.

Submission:

Contributions should be sent to the Editor before the annual deadline (November 30th) for each issue. Contributions submitted after this date will be returned. Colour illustrations are welcome. Contributions should be submitted both in hardcopy (THREE complete copies) to the Editor and in electronic format to m.shotton@dl.ac.uk. Text should be in Word 6 format and illustrations should be submitted as separate files in TIFF format. The December 1998 edition of *Fibre Diffraction Review* should be used as a style-guide and can be viewed at: http://www.clrc.ac.uk/Publications/FibreDiffractionReview/Issue7/index.asp

Reprints:

Currently it is cheaper to reproduce the whole Journal than to prepare separate reprints of each article. Those wishing to purchase multiple extra copies of the Journal at the prices detailed below should specify this when their article is submitted. Non-contributors who wish to purchase extra copies of the Journal may do so on the same terms as above by contacting the Editor before the November 30th deadline.

Extra copies:

1 copy	£5
5 copies	£22
10 copies	£40
20 copies	£70
30 copies	£90
50 copies	£125
100 copies	£200

(prices include postage and packing)

Editor's Address:

Professor John M. Squire,
Editor, *Fibre Diffraction Review*,
Biological Structure and Function Section,
Biomedical Sciences Division,
Imperial College of Science, Technology and Medicine,
London SW7 2AZ.

e-mail: j.squire@ic.ac.uk
voicemail: 0207 594 3185
FAX: 0207 594 3169

9th Annual Fibre Diffraction and Non-Crystalline Diffraction Workshop

26th-28th June 2000

University of Sheffield

Speakers include:

F.	Bates	Minnesota, U.S.A.
W.	Bras	E.S.R.F., France
J.	Higgins	Imperial, U.K.
M.	Irving	Kings, U.K.
P.	Lindner	I.L.L., France
R.	Millane	Purdue, U.S.A.
S.	Perkins	Royal Free Hospital, U.K.
A.	Ryan	Sheffield, U.K.
G.	Stubbs	Vanderbilt, U.S.A.
Y.	Nishiyama	Tokyo, Japan
T.	Irving	Illinois, U.S.A.
D.	Myles	E.M.B.L., France
M.	Muller	E.S.R.F., France
T.	McLeish	Leeds, U.K.
D.	Svergun	E.M.B.L., Germany
G.	Tiddy	U.M.I.S.T., U.K.
R.	Richardson	Bristol, U.K.
M.	Leaver	Lancashire, U.K.
R.	Cameron	Cambridge, U.K.
M.	Shotton	Daresbury Laboratory, U.K.

+ Hands-on demonstration of CCP13 and NCD software

For further information and registration, see the web pages at http://www.dl.ac.uk/SRS/CCP13 or contact m.shotton@dl.ac.uk

(supported by CCP13, DARTS and Daresbury Laboratory)

Useful World Wide Web addresses (URL)

CCP13	http://www.dl.ac.uk/SRS/CCP13
NCD	http://www.srs.dl.ac.uk/NCD
SRS	http://www.srs.dl.ac.uk
DARTS	http://www.srs.dl.ac.uk/DARTS

ISSN 1463-8401